Chem Soc Rev

This article was published as part of the

2008 Gold: Chemistry, Materials and Catalysis Issue

Please take a look at the full table of contents to access the other papers in this issue

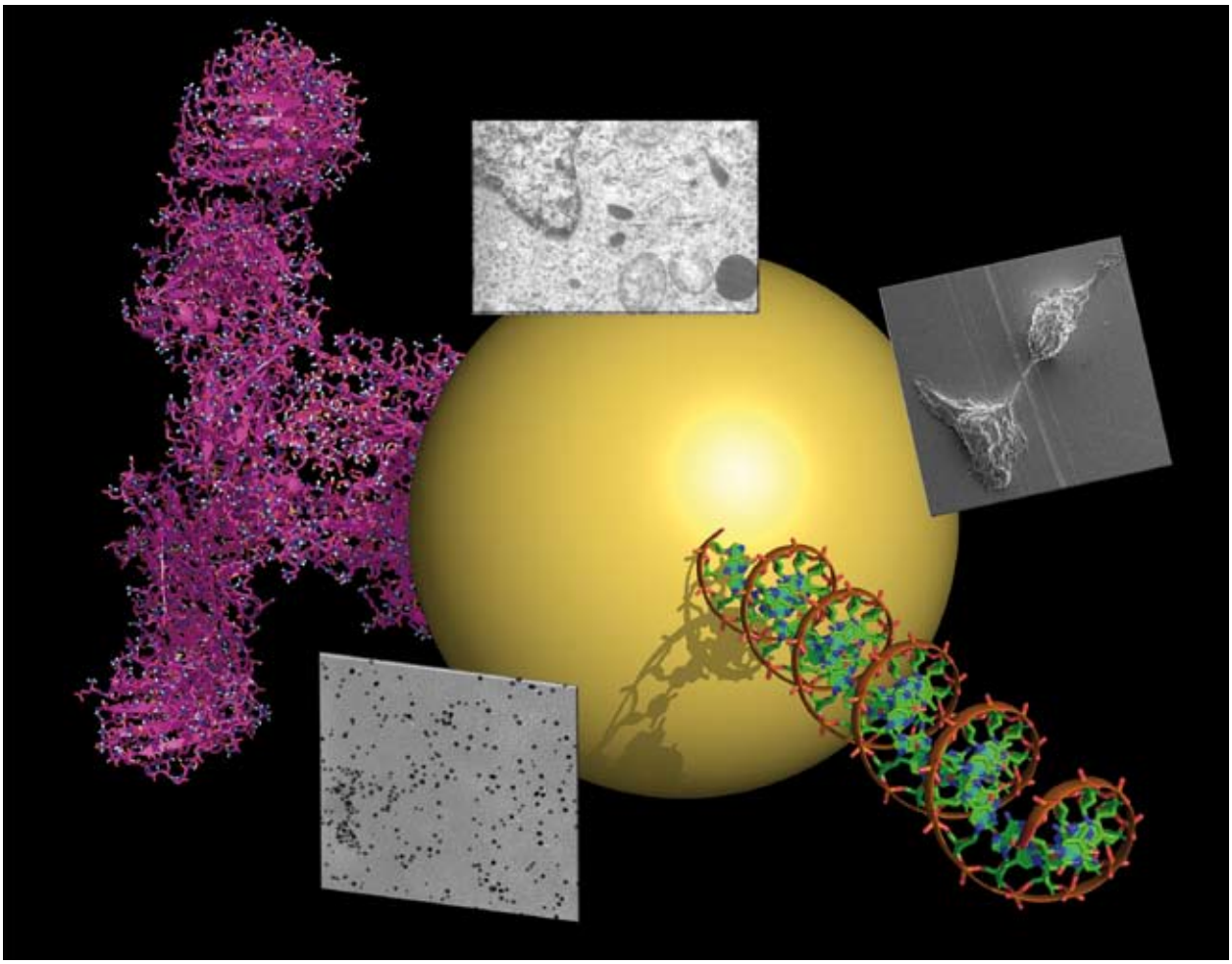

The relevance of shape and size of Au_{55} clusters†

Günter Schmid*

Received 7th February 2008
First published as an Advance Article on the web 2nd July 2008
DOI: 10.1039/b713631p

This *critical review* deals with the history of $Au_{55}(PPh_3)_{12}Cl_6$ and its derivatives from the very beginning in 1981 to date. Au_{55} clusters obtain their special interest from their ultimate size and their ideal cuboctahedral structure. They are part of the family of so-called full-shell clusters, particles with perfectly completed geometries, also represented by icosahedral Au_{13} clusters. Bare as well as ligand protected Au_{55} clusters not only exhibit special chemical and physical stability, but draw their attention particularly from their unique electronic properties. Single electron switching at room temperature becomes possible, giving rise for development of applications in future nanoelectronic devices. A predominantly size-determined property of the 1.4 nm particles becomes obvious with respect of biological response. Au_{55} clusters indicate an unusual cytotoxicity which seems to be caused by the unusually strong interaction between the 1.4 nm particles and the major grooves of DNA. Only marginally smaller or larger particles show drastically reduced toxicity, whereas significantly larger gold nanoparticles are completely non-toxic. Both, the electronic perspectives as well as the relevance in toxicology are at very early stages of development (75 references).

1. Introduction

More than 25 years after its discovery[1] the scientific story of the gold cluster compound $Au_{55}(PPh_3)_{12}Cl_6$ is reviewed in the following article. Among the huge number of gold nanoparticles that have been generated and investigated in the meantime, $Au_{55}(PPh_3)_{12}Cl_6$ and a series of derivatives hold a very special place. The reason for that is the monodispersity, the full-shell character (see below) and the size of the Au_{55} nucleus of 1.4 nm, from which unique electronic properties are followed. Larger gold nanoparticles, also called gold colloids, are known since centuries and have been and still are used to colour glass (ruby glass). Systematically, gold colloids were synthesized and investigated for the first time by Michael Faraday in the 19th Century.[2] In the meantime, numerous synthetic procedures have been developed and gold nanoparticles are now available in the size range from *ca.* 1 nm up to several hundred of nanometres. Except a few examples, they all are characterized by more or less broad size distributions and imperfect structures. This statement explicitly excludes numerous gold clusters <1 nm with molecular character, consisting of a distinct number of gold atoms and usually fully characterized by X-ray structure analyses. The term ''nanoparticle'' generally is used for particles >1 nm of inexact size and structure, whereas the term ''cluster'' should be restricted to stoichiometrically exact species. However, it has to be noticed that this differentiation is not consequently followed in the literature. Frequently, the term ''nanocluster'' is also used, meaning something between the both exponents. Two recent reviews on gold nanoclusters and nanoparticles present the state of the art of this still rapidly growing field of nanoscience.[3,4]

On the way from simple gold complexes to Au_{55} an impressive list of structurally characterized gold clusters has become known. Only few examples shall be mentioned here. The Au_8 core in the cluster $Au_8(PPh_3)_7(NO_3)_2$ forms an incomplete icosahedron,[5] just like the Au_9 nucleus in $Au_9[P(C_6H_4\text{-}p\text{-}Me)_3]_8(PF_6)_3$[6] or its BF_4^- derivative.[7] This series can be continued by the example $Au_{10}Cl_3(PCy_2Ph)_6NO_3$ (Cy = cyclohexyl), the Au_{10} core of which is however, not characterized by a fragmentary icosahedron, but shows approximately D_{3h} symmetry and can be described as a hexagonal ring of six edge- and face-sharing tetrahedral atoms with a central Au atom.[8]

Universität Duisburg-Essen, Institut für Anorganische Chemie, Universitätsstrasse 5-7, Essen, 45117, Germany. E-mail: guenter.schmid@uni-due.de

† Part of a thematic issue covering the topic of gold: chemistry, materials and catalysis.

Günter Schmid

Günter Schmid received his Doctor's degree in Inorganic Chemistry at the University of Munich. His Habilitation was performed at the University of Marburg where he received a Professorship in 1971. From 1977–2002 he worked as the Director of the Inorganic Chemistry Department at the University of Essen. His main research interests include the generation and investigation of large metal clusters and nanoparticles. The biological responses to metal nanoparticles is another field of interest. He has published ca. *350 papers, edited five books on nanoscience and -technology, and received the Wilhelm Klemm Award from the German Chemical Society.*

Nevertheless, the relationship to the icosahedral structure becomes visible. The first Au_{11} cluster was reported already in 1969, as part of the compound $Au_{11}(PPh_3)_7(SCN)_3$,[9] followed by other Au_{11} species in 1970[10] and 1972.[11] A "natural" end of this continuous development was the synthesis of some Au_{13} species. Perfect icosahedra, for instance in the cluster $Au_{13}(dppm)_6(NO_3)_2$ (dppm = $Ph_2P–CH_2–CH_2–PPh_2$),[12] were detected.

Beyond Au_{13}, a less perfect row of gold cluster compounds has been discovered. One structurally fully characterized species should be mentioned: $[Au_{39}(PPh_3)_{14}Cl_6]Cl_2$.[13] This cluster compound, having the threefold amount of Au atoms, shows nature's tendency to form densely packed structures if the number of building blocks, here the Au atoms, increases. The gold atoms in Au_{39} are arranged in a slightly distorted hexagonal close packed manner. Icosahedra are less dense packed structures, due to their five-fold symmetry. However, in this connection it should be mentioned, that the structures of metal rich compounds not only depend on the number of metal atoms, but also on the number and nature of protecting ligands.

Very recently, a big jump in the development of structurally defined gold clusters has been made by the synthesis and investigation of Au_{102}(*p*-MBA)$_{44}$ (MBA = *p*-mercaptobenzoic acid).[14] The structure of the gold core is described to consist of a rather complex arrangement of fcc, hcp, icosahedrally and decahedrally arranged inner atoms. It can be assumed that this unique structure is substantially influenced by the special nature of the mercaptobenzoic acid ligands, forming not only very strong Au–S bonds, but also interact *via* the carboxylic functions with one another to form a rigid and very stable shell around the 102 gold atoms. This special situation may also be the reason for the crystallizability of this compound. As will be discussed later, weakly bound ligands like in $Au_{55}(PPh_3)_{12}Cl_6$, partially dissociate in solution and so give rise for the formation of strong Au–Au interactions, ending up in cluster aggregates.

The clearing up of the atomic arrangement in Au_{55} by single-crystal X-ray analysis was not possible so far. As already indicated, the comparatively weak Au–P bonds in $Au_{55}(PPh_3)_{12}Cl_6$ do not allow extended crystallisation procedures due to decomposition. On the other side, microcrystalline material has easily been obtained and could be used for X-ray powder diffraction experiments. The lack of large single crystals was, on the other hand, the reason for the application of all relevant physical methods to gain information not only on structural details, but at the same time on numerous other properties.

The lack of a single-crystal X-ray structure analysis of $Au_{55}(PPh_3)_{12}Cl_6$ or one of its derivatives was occasionally the reason for doubts concerning its size and structure, not only by other groups, but also by ourselves. However, meanwhile there exist so many indications for the correctness of the formula that doubts seem no longer justified. Many groups around the world used and still use Au_{55} clusters for various investigations, one derivative is commercially available. The assumption that $Au_{55}(PPh_3)_{12}Cl_6$ is a single chemical compound results not only from its monodispersity, but follows from molecular weight determinations and elementary analyses which are performed from any prepared sample.

The present review deals with the phenomenon of full-shell clusters, especially those of gold, their formation and organization in different dimensions and with the behaviour of ligand-free Au_{55} clusters, followed by the discussion of the unique electronic properties of Au_{55} cluster compounds as well as of aspects of future applications. Beyond that, fascinating new developments will be considered, namely the interaction of Au_{55} clusters with bio-systems. The biological responses to Au_{55} are, compared with that of larger and smaller gold nanoparticles, absolutely surprising and of general relevance.

2. Full-shell clusters

The expression "full-shell cluster" comprises particles composed of a central atom, regularly surrounded by individual shells of atoms and ending up in perfect outer geometries. In principle, full-shell clusters could be based on icosahedra, but they are less favoured for larger particles due to their lower density compared with *e.g.* a hexagonal close packed (hcp) arrangement, as is observed in most transition metals, among others in bulk gold. A central atom is coordinated by 12 others as a maximum in the 1st shell, followed by 42 in the 2nd shell, *etc*. In general, the construction follows the relation: number of atoms per shell = $10n^2 + 2$, with n = shell number. The total number of atoms for a distinct full-shell cluster is given by 1 + 12 = 13 (one-shell cluster), 13 + 42 = 55 (two-shell cluster), 55 + 92 = 147 (three-shell cluster) *etc*. in close-packed arrangements forming perfect cuboctahedra. Fig. 1 illustrates the formation of full-shell clusters up to a four-shell cluster consisting of 309 atoms.

The special stability of full-shell clusters was demonstrated for the first time by Recknagel and co-workers in 1981, using xenon atoms.[15] Supersaturated Xe gas was expanded into a mass spectrometer and in a continuous row of signals, maxima for Xe_{13}, Xe_{55} and Xe_{147} were observed. This was interpreted by the formation of especially stable and long-lived full-shell clusters. Meanwhile there exists a series of transition metal full-shell clusters, beginning with Au_{13} (icosahedral), Rh_{13} (cuboctahedral),[16] Rh_{55},[17] Au_{55},[1] Pt_{309} (four-shell),[18] Pd_{561} (five-shell),[19] Pd_{1415} (seven-shell)[20] and even Pd_{2057} (eight-shell),[20] all cuboctahedral. In this connection it should be mentioned that all these clusters are equipped with a shell of appropriate ligand molecules for at least two reasons: synthesis generally happens in solution *via* metal atoms and requires surface protecting molecules to stop uncontrolled particle growth and to prevent metal–metal interactions with coalescence. Furthermore, it should also be stated that at least the five-, seven- and eight-shell clusters may deviate to some extent from an ideal stoichiometry. Nevertheless, from high-resolution transmission electron microscopy (HRTEM), the full-shell nature of these giant clusters can be followed, as is shown in Fig. 2 by two examples.

The four-shell cluster Pt_{309} (a) consists of a central plane (a row) of atoms, involving the central atom, and four additional planes on each side. The eight-shell cluster Pd_{2057} altogether shows 17 planes (b) (1 + 8 + 8).

2.1 Formation of ligand-protected Au_{13} and Au_{55} clusters

First of all it should be mentioned that the aimed synthesis of distinct full-shell clusters is still not possible. Rather they are found by chance and the experience of the experimentalist. Of course, if a synthetic route has been found for the first time, reproducibility is a condition. The only working procedure to

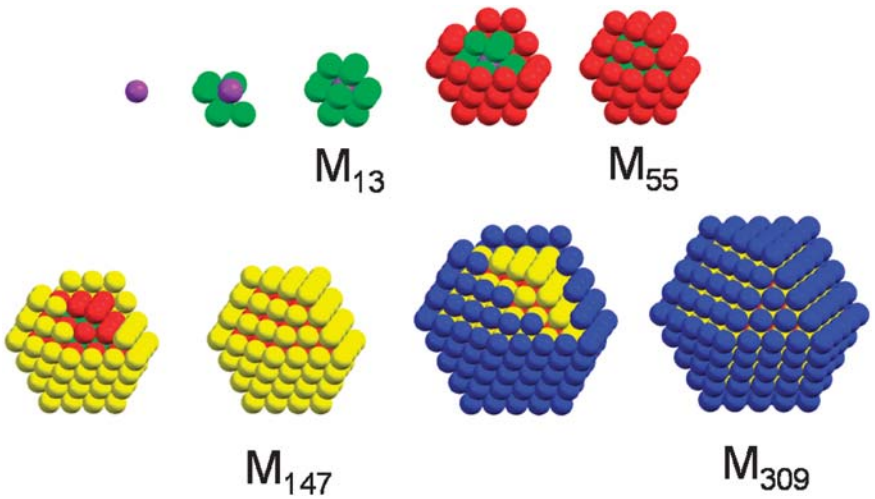

Fig. 1 Organization of full-shell clusters: a first single atom (purple) is surrounded by 12 others (green) to give a one-shell cluster M_{13}. 42 atoms (red) can be densely packed on the 12 green atoms ending with the M_{55} two-shell cluster, followed by 92 atoms (yellow) and 162 atoms (blue) to give M_{147} and M_{309}, respectively.

synthesize gold full-shell clusters up to date uses reduction of gold salts in the presence of appropriate ligand molecules in solution. The icosahedral one-shell cluster $Au_{13}(dppm)_6(NO_3)_4$ (dppm = $Ph_2CH_2CH_2PPh_2$), mentioned above, was synthesized from $Au_2(dppm)(NO_3)_2$ and $NaBH_4$.[12] The chelating dppm molecules trap the Au_{13} clusters and stabilize them in such a manner that further growth is prevented. A stepwise synthesis is also possible, as is shown with $[Au_{13}(PMe_2Ph)_{10}Cl_2](PF_6)_3$.[21] It is formed of $[Au_{11}(PMe_2Ph)_{10}]^{3+}$ and Et_4NCl in alcoholic solution. The mechanism of this surprising reaction is still unknown.

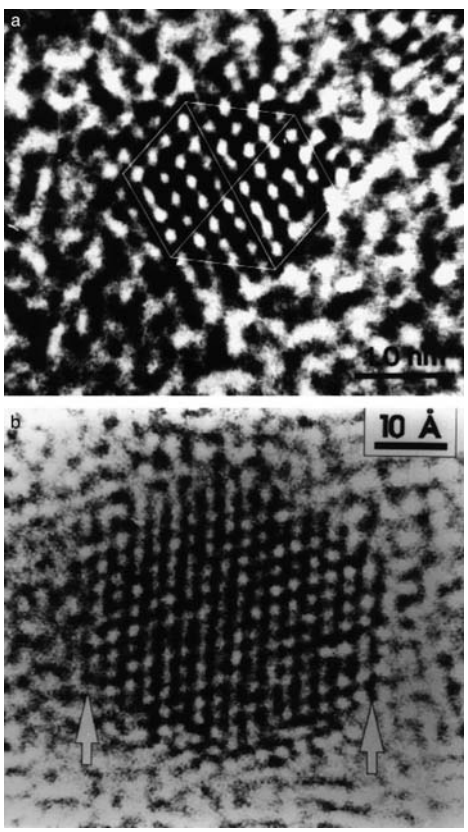

Fig. 2 HRTEM images of full-shell clusters. (a) four-shell cluster Pt_{309}, (b) eight-shell cluster Pd_{2057}. 9 (1 + 4 + 4) atomic planes in Pt_{309} and 17 (1 + 8 + 8) planes in Pd_{2057} can be counted. ((a) Reprinted with permission from ref. 18. Copyright 1989, Wiley-VCH, (b) Reprinted with permission from ref. 20. Copyright 1993, American Chemical Society.)

The synthesis of the first Au_{55} cluster goes back to the same year, 1981, when the first Au_{13} clusters were found. Ph_3PAuCl, dissolved in benzene or toluene, was treated with gaseous B_2H_6 at 60 °C to form $Au_{55}(PPh_3)_{12}Cl_6$ in about 30% yield.[1,22] Several attempts to use $NaBH_4$ instead of diborane as reducing agent failed, and the reasons can satisfactorily be understood. One function of B_2H_6 is to reduce Au(I) in the starting compound to Au(0), apart from the six Au atoms linked to chlorine atoms and so having the formal oxidation state +1. The other, and probably decisive function, is its ability to bind excess PPh_3 as $Ph_3P–BH_3$, a Lewis base–Lewis acid adduct. This is not possible if $NaBH_4$ is used. Experimental and analytical details, especially the separation from other products and further purification, will not be discussed here. Solid $Au_{55}(PPh_3)_{12}Cl_6$ forms a microcrystalline, dark brown powder, best soluble in dichloromethane. Solutions of the cluster are only of limited stability due to partial dissociation of PPh_3 ligands. Dissociation of ligands in solution is a well known phenomenon in complex chemistry and usually leads to stable equilibria. However, if there is an alternative for the ligand deficient species, the equilibrium will be disturbed. In case of $Au_{55}(PPh_3)_{12-x}Cl_6$ the formation of stable gold–gold contacts, eventually leads to insoluble aggregates. As a consequence, solutions of the cluster have to be used as fast as possible after generation to avoid such unwanted reactions. However, chemical reactions, for instance ligand exchange reactions, can be performed in the course of a couple of hours or even days without visible decomposition, due to the presence of excess new ligand molecules. On the contrary, in the solid state, the cluster is indefinately stable at room temperature or below. From *ca.* 60 °C on, decomposition starts. The rather weak Au–P bonds in solution have been studied by ^{31}P NMR spectroscopy.

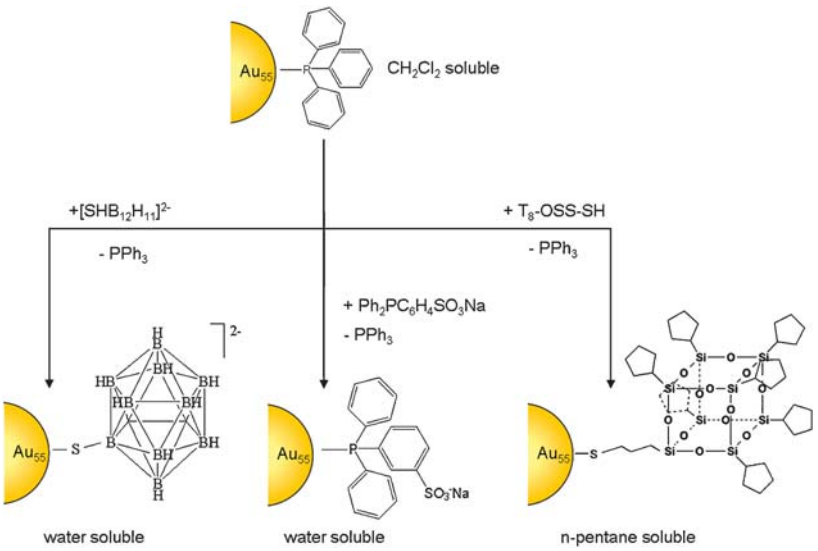

Fig. 3 Substitution of PPh_3 in $Au_{55}(PPh_3)_{12}Cl_6$ by other ligands, generating hydrophilic or hydrophobic character.

Addition of excess PPh_3 to $Au_{55}(PPh_3)_{12}Cl_6$ solutions results in single, averaged ^{31}P signals, the shift of which depends on the amount of additional phosphines. The ligand exchange is faster than the NMR time scale; the calculated contact time is $\tau = 3.0 \pm 0.5$ μs.[23]

The labile Au–PPh_3 bond can be used for ligand exchange reactions resulting in various derivatives. Whereas the original compound $Au_{55}(PPh_3)_{12}Cl_6$ is soluble in CH_2Cl_2, the solubility can be tuned by changing the nature of the ligand shell from hydrophilic to hydrophobic. Fig. 3 informs on some exchange reactions and the different solubilities of the products.

The substitution of PPh_3 by the monosulfonated derivative $Ph_2PC_6H_4SO_3Na$ succeeds best by a phase transfer reaction from CH_2Cl_2 into water, containing the sulfonated ligand.[24] The phase transfer shifts a possible equilibrium state with both ligand types quantitatively to the water soluble cluster derivative. Na^+ can easily be exchanged by H^+ *via* ion exchange.

Another water-soluble cluster is obtained using the *closo*-borate $Na_2[B_{12}H_{11}SH]$ to exchange PPh_3, also by a phase-transfer reaction and by generating stable Au–S bonds.[25] As has been found, about six phosphine ligands are substituted in a couple of days, the total exchange takes about 6 weeks! The reason for that time-consuming reaction is to be seen in the accumulation of negative charges by the doubly charged $[B_{12}H_{11}SH]^{2-}$ ions, inducing increasing Coulomb repulsion. Interestingly, the Na^+ ions can be exchanged by $[N(octyl)_4]^+$ in a reverse phase transfer reaction, resulting in $Au_{55}\{(B_{12}H_{11}SH)[N(octyl)_4]_2\}_{12}Cl_6$ which is again soluble in CH_2Cl_2.[25]

A derivative with a totally nonpolar surface is created when PPh_3 is substituted by the silsesquioxane $(cyclopentyl)_7Si_8O_{12}(CH_2)_3SH$ (T_8-OSS-SH), the structure of which can be seen from Fig. 3.[26] The quantitative exchange is again facilitated by the formation of strong Au–S bonds. Due to the cyclopentyl substitutents in T_8-OSS-SH the nonpolar character is transferred to the cluster which is now very soluble in *n*-pentane.

These experiments impressively demonstrate that solubility of nanoparticles strictly depends on the nature of the protecting ligand shell and can be varied from hydrophilic to hydrophobic.

It is important to remark that the size of the cluster nucleus in all these reactions did not change. As an example, a TEM image of the silsesquioxane derivate is shown in Fig. 4, indicating the monodispersity of the particles in an extended area with randomly oriented clusters (A) and in a magnified cutout of a two-dimensionally ordered arrangement (B).

A very special kind of ligand exchange has recently been reported: the total coverage of the Au_{55} nucleus by a single dodecadentate thioether.[27] For this, the synthesis of the ligand molecule, shown in Fig. 5, had first to be developed. The ligand exchange at $Au_{55}(PPh_3)_{12}Cl_6$ succeeded by means of a phase-transfer reaction into water without changing the cluster size.

All 12 PPh_3 ligands at the 12 corners of the cuboctahedron become substituted by the 12 thiol functions of the dodecadentate molecule, increasing its kinetic and thermal stability remarkably. Thermal stability tests have been performed by binding the cluster to a 5′-thiol-modified 27 mer with a 3′-fluorescein functionalized complementary strand. In case of having an intact cluster in the neighbourhood of the fluorescence marker, fluorescence is quenched. Indeed, during 100 warming–cooling cycles between 20 to 95 °C the fluorescence is quenched at 20 °C, but reappears at 95 °C due to the separation of the complementary strands. Less than 10% of the clusters are destroyed during the first 100 min. This experiment clearly demonstrates the importance of a protecting ligand shell concerning stability of the nanoparticles.

2.2 Organisation of ligand-protected Au_{55} clusters

The generation of three- (3D), two- (2D) and one-dimensionally (1D) organized ligand protected Au_{55} clusters has been intensively investigated during the last decade. 3D organization, usually simply called crystallization, happens by itself under appropriate conditions from solution. However, as has been mentioned before, the generation of larger crystals of $Au_{55}(PPh_3)_{12}Cl_6$ failed due to the fast decomposition of the

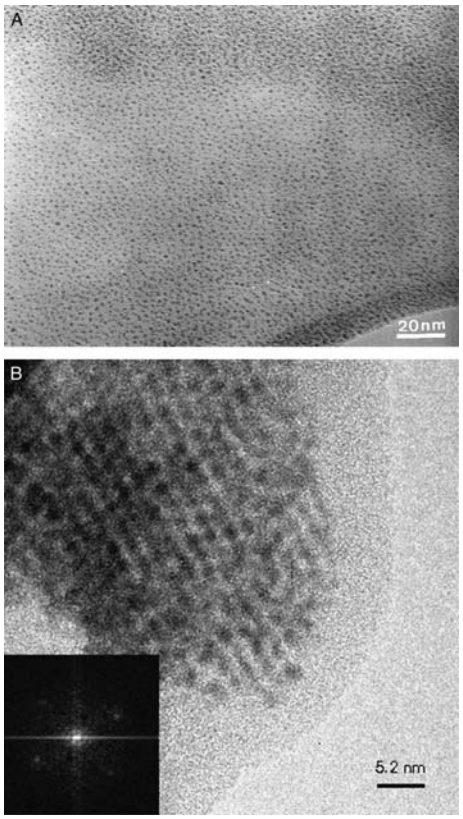

Fig. 4 TEM image of an extended area of $Au_{55}(T_8\text{-OSS-SH})_{12}Cl_6$ clusters, deposited on a TEM grid from solution (A) and a small area of ordered clusters formed by chance (B). (Reprinted with permission from ref. 26. Copyright 1998, Wiley-VCH).

clusters in solution. The crystallisation of more stable derivatives, as discussed in section 2.1, has so far not yet been object for experiments, but should be more promising compared with the parent compound. In spite of the lack of larger crystals, 3D arrangements of $Au_{55}(PPh_3)_{12}Cl_6$ in the micrometer regime have been successfully investigated by means of TEM and X-ray powder diffraction.

2.2.1 3D Organisation. Micrometer sized crystals of $Au_{55}(PPh_3)_{12}Cl_6$ clusters are formed from concentrated dichloromethane solution in preparative amounts by fast evaporation of the solvent. Well shaped microcrystals are observed by TEM, as can be seen in Fig. 6.[28] Fig. 6(a) shows crystals of rather the same size and from the magnified cutout in Fig. 6(b) the perfect arrangement of hexagonally close-packed clusters can be followed. The separation between the cluster rows is *ca*. 2.0–2.1 nm. Assuming an fcc arrangement of the clusters, the distance corresponds to an effective cluster distance of 2.3–2.4 nm, in agreement with the calculated cluster diameter considering van der Waals distances between the PPh_3 ligands.

Small-angle X-ray diffraction (SAXRD) experiments resulted in only one strong reflection of $2\theta = 4.3^\circ$, corresponding to a *d* value of 2.05 nm, in perfect accord with the HRTEM result, and a hexagonal close-packing, if observed along the [111] direction.[28]

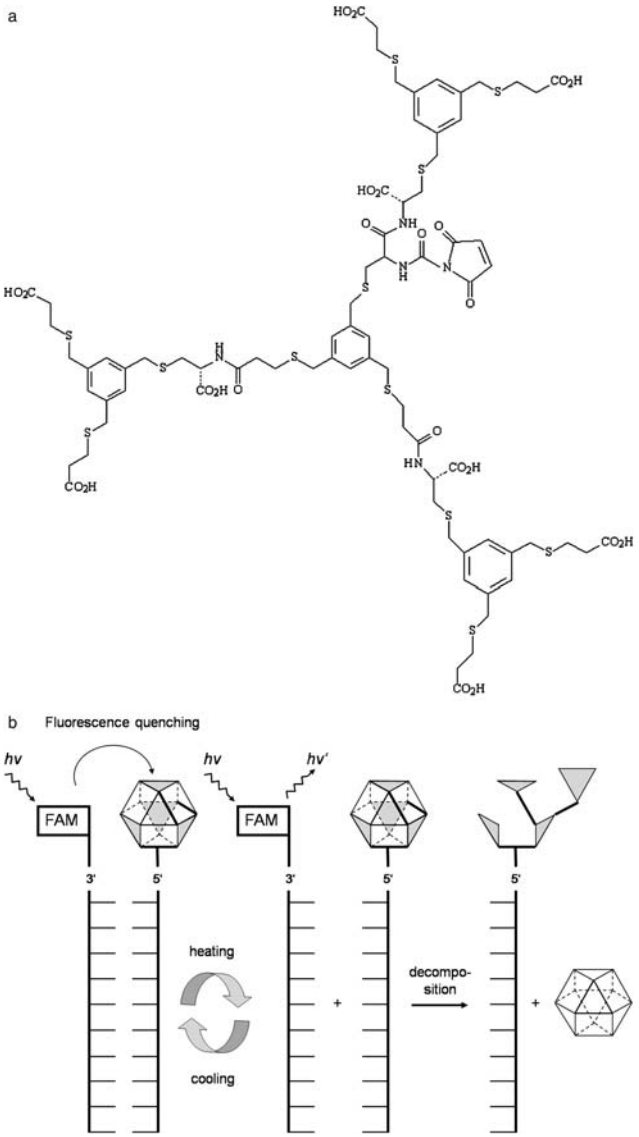

Fig. 5 (a) The dodecadentate thioether molecule used to completely capture the Au_{55} cluster. (b) Sketch of the heating and cooling processes with separation and recombination of the complementary strands and final decomposition of the complex (FAM = fluorescein-aminomodifier). The four linked (bold lines) grey triangles in the cuboctahedra indicate the presence of the four tridentate 1,3,5-tris (mercaptomethyl)benzene units of the decadentate ligand molecule.

2.2.2 2D Organisation. Ordered monolayers of ligand protected Au_{55} clusters can be generated on different routes. Islands of $Au_{55}(PPh_3)_{12}Cl_6$ can easily be prepared on water surfaces from thin films of cluster solutions. Evaporation of the solvent generates relatively small areas of hexagonally and quadratically organized clusters on the water surface where they can be transferred from to substrates.[29]

A condition to organize the particles in a reasonable extension is a weak interaction with the surface. On the one hand, there should be an attraction towards the clusters in solution, on the other hand there must be sufficient mobility for deposited particles to organize themselves.

$Au_{55}(PPh_3)_{12}Cl_6$ organizes in two different packing modes on a poly(vinylpyrrolidone) (PVP) film at the phase boundary

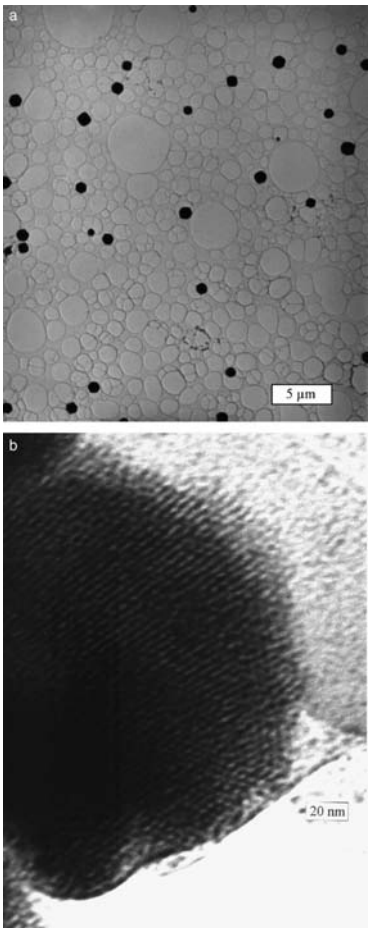

Fig. 6 Microcrystals of $Au_{55}(PPh_3)_{12}Cl_6$ (a) and high resolution image of a thin crystal part indicating the highly ordered cluster layers (b). (Reprinted with permission from ref. 28. Copyright 1999, Royal Society of Chemistry.)

of water and dichloromethane.[30] Usually, a hexagonal order dominates, however, square orders form more extended areas. The reason for the formation of both modifications is to be seen in the type of the very first and accidental contacts between cluster molecules. The function of the PVP, dissolved in the water phase, can be seen in weak hydrophobic–hydrophobic interactions between the polyvinyl backbone and the phenyl rings of the clusters.

The acidified derivative $Au_{55}(Ph_2PC_6H_4SO_3H)_{12}Cl_6$ self-assembles on thin films of poly(ethyleneimine) (PEI), generated, for instance, on the carbon film on a TEM copper grid. The reason for the organized self-assembly is the interaction between the SO_3H functions and the NH groups of PEI. Again, hexagonal close packed and square structures are observed. Fig. 7 shows a cutout of perfectly organized clusters of square order.[31]

2.2.3 1D Organisation. Generally, one-dimensional organisation of nanoparticles is difficult and only few examples of perfect 1D arrangements have become known. Nature tends to organize in more than one dimension and so generation of 1D structures requires technical assistance.

A quasi-1D structure of $Au_{55}(PPh_3)_{12}Cl_6$ has been generated by a rather exotic method, namely the controlled degradation of

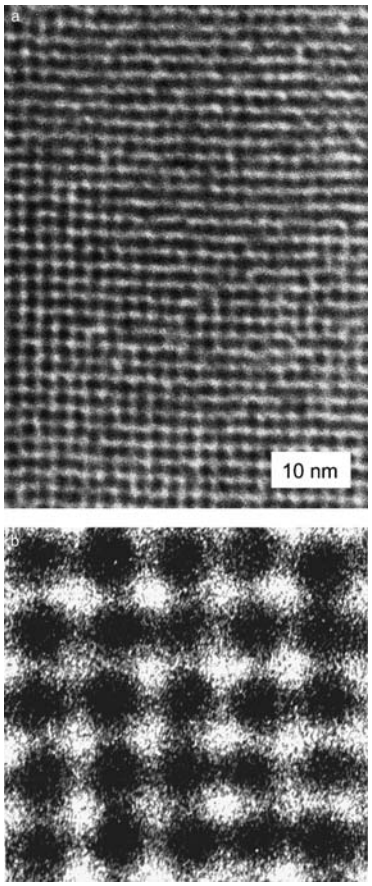

Fig. 7 (a) TEM image of a square ordered monolayer of $Au_{55}(Ph_2PC_6H_4SO_3H)_{12}Cl_6$ on a PEI film. (b) magnified cutout. (Reprinted with permission from ref. 31. Copyright 2000, Wiley-VCH.)

ordered cluster monolayers.[32] If islands, swimming on a water surface (see above), are transferred to smooth solid substrates under strictly controlled conditions, for instance under a 20° withdrawal angle and a computer controlled speed of 10 cm min^{-1}, the oscillation of the water meniscus at the water-substrate boundary "cuts" the islands into stripes of 3–4 cluster rows. Fig. 8 shows a TEM image of such an assembly of cluster rows.

Strictly one-dimensional cluster arrangements have become accessible by a particular technique, based on the chemical modification of an alkyl-terminated self-assembled monolayer.[33–36] Specific oxidation of terminal CH_3 groups by a metalized AFM tip, inducing electric pulses, results in the generation of COOH functions which then can be functionalized by SH groups, strongly binding Au_{55} clusters by substitution of PPh_3 molecules. The process is sketched in Fig. 9. Fig. 10 shows an AFM image of two 1D cluster rows, intentionally interrupted to deposit individual clusters.

Depending on the software of the atomic force microscope, any kind of pattern can be drawn by this technique.

2.3 Generation and organisation of bare Au_{13} and Au_{55} clusters

The nature of full-shell clusters suggests a special stability due to their perfect outer geometry. Indeed, if the protecting

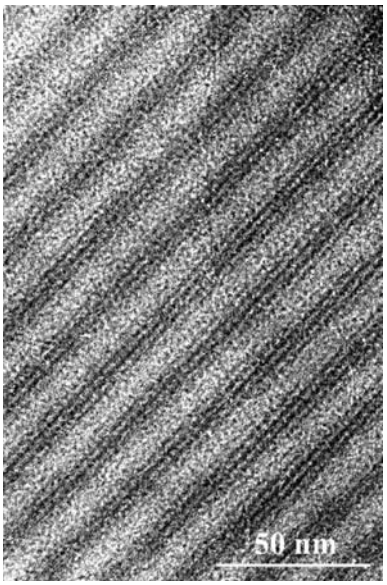

Fig. 8 TEM image of stripes of cluster rows, generated by artificial degradation of ordered monolayers. (Reprinted with permission from ref. 32. Copyright 2001, Royal Society of Chemistry).

ligands are removed under mild conditions, naked Au_{13} as well as Au_{55} clusters can be generated and their behaviour can be studied under appropriate conditions.

The first indication of the existence of ligand-free Au_{13} clusters was observed already in 1986.[37] Electrophoresis of dichloromethane solutions of $Au_{55}(PPh_3)_{12}Cl_6$ resulted in the removal of the outer shell of gold atoms with formation of $(PPh_3)_2AuCl$, bulk gold and a species $(Au_{13})_x$. X-Ray powder diffraction investigations resulted in a unique structural situation: bare Au_{13} clusters first organize to $(Au_{13})_{13}$, full-shell clusters of full-shell clusters, which then behave as building blocks for microcrystals of the general formula $[(Au_{13})_{13}]_n$. This result was the first indication that bare full-shell clusters interact with each other in an organized manner and not simply to give a polycrystalline material.

The fact that ligand-protected Ru_{55} and Rh_{55} clusters behave in the same manner[37] supports the generality of this observation.

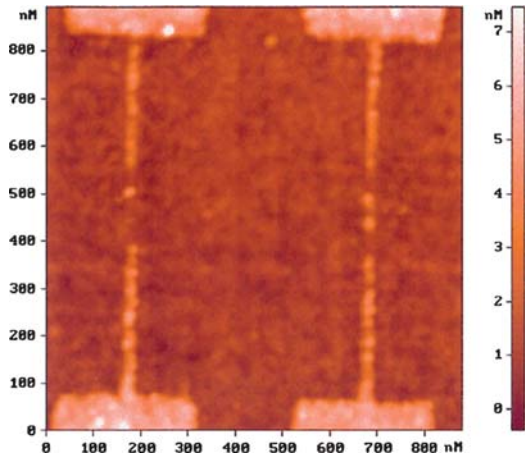

Fig. 10 AFM image of strictly one-dimensionally ordered $Au_{55}(PPh_3)_{12-x}Cl_6$ clusters. The 1D wires are intentionally interrupted to deposit one (left) and two (right) individual clusters. (Reprinted with permission from ref. 36. Copyright 2002, American Chemical Society).

The results with $Au_{55}(PPh_3)_{12}Cl_6$ have been indirectly confirmed by a totally different experiment.[38] Secondary ion mass spectrometry (SIMS) has been applied for mass determination of the cluster. Instead, degradation to Au_{13} clusters was observed which organize, even under the unusual conditions in the spectrometer, to multiples $(Au_{13})_n$ with maxima at $n =$ 15, 23, 31, 39, 47 and 55. $(Au_{13})_{55}$ is the continuation of $(Au_{13})_{13}$, a full-shell cluster of full-shell clusters!

How can bare Au_{55} clusters be generated? Under mild conditions, a rather strange route turned out to work best: the removal of the PPh_3 ligand molecules by the thiol terminated dendrimer G4-SH which is shown in Fig. 11.[39]

In cluster solutions with excessive dendrimer, the PPh_3 ligands are removed by the thiol functions of the spherical dendrimer. However, due to the excessive dendrimer molecules, the clusters can move around on the dendrimer surface, since all positions are equivalent. Finally, bare clusters meet from time to time and touch each other with formation of stable metal–metal bonds inside of a cavity of dendrimers. Fig. 12 illustrates the process formally.

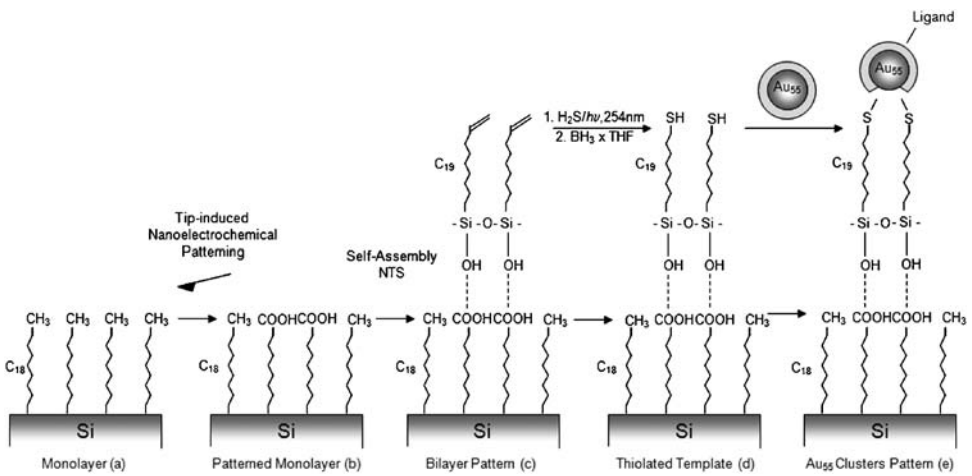

Fig. 9 Generation of thiol-functionalized molecular monolayer to bind Au_{55} clusters.

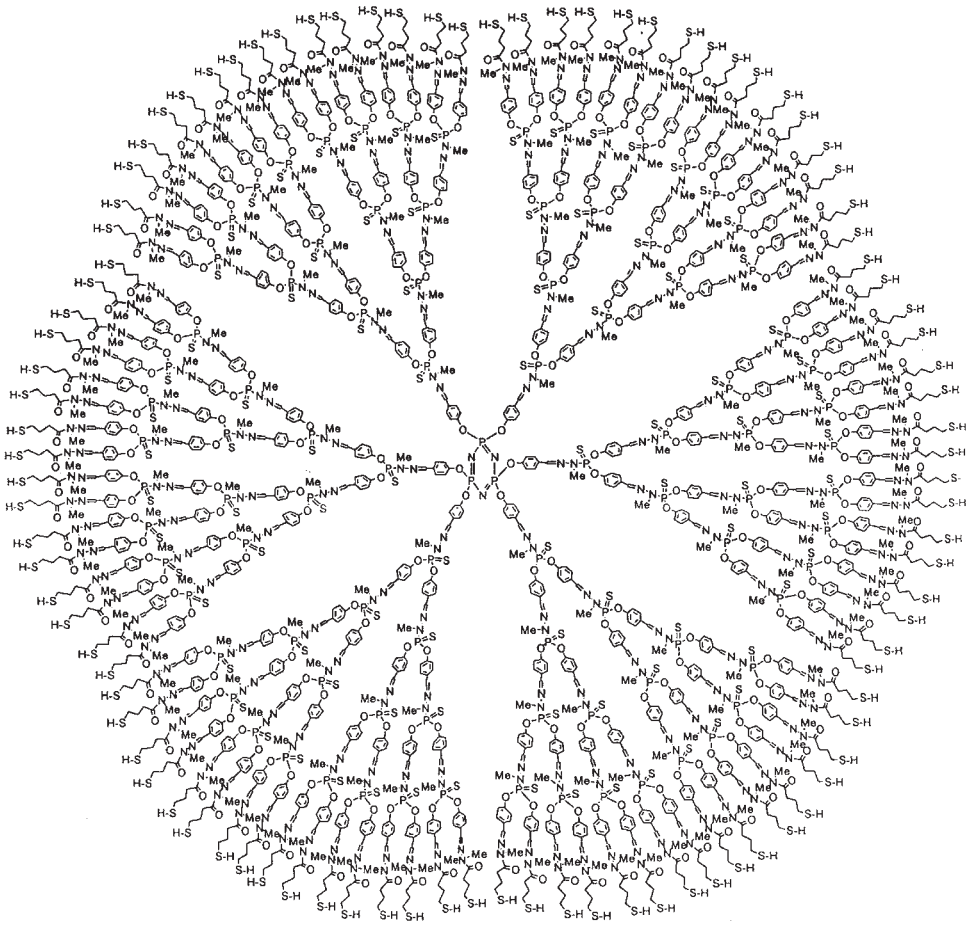

Fig. 11 The fourth-generation dendrimer G4-SH with 96 SH end-groups.

It seems surprising that this aggregation of Au_{55} particles happens in an ordered manner, resulting in partially well-shaped microcrystals that have been characterized by TEM and X-ray powder diffraction. Fig. 13 shows one of the perfect crystals, a TEM cutout of a thin border area together with a sketch of the ordering principle as it results from TEM and X-ray data.

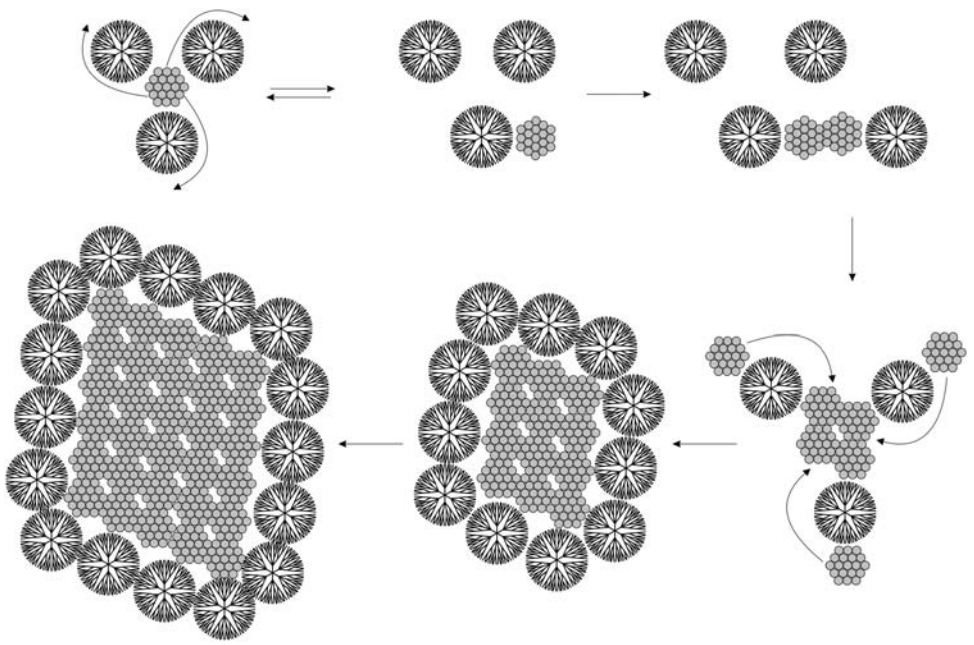

Fig. 12 Illustration of formation of microcrystals of bare Au_{55} clusters inside a cavity of G4-SH.

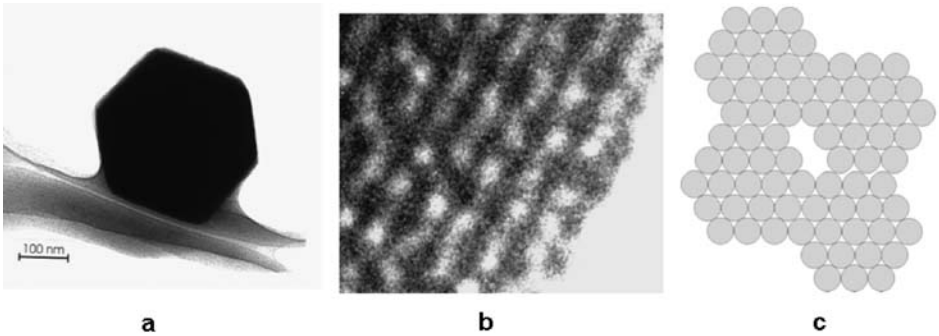

Fig. 13 A microcrystal of bare Au_{55} in a shell of G4-SH dendrimers (a). A TEM image of a cutout of a thin crystal border area shows the cluster arrangement (b) which is sketched in (c) for clearness. ((a), (b) Reprinted from ref. 39. Copyright 2000, Wiley-VCH).

The destiny of the chlorine atoms during this process is somewhat unclear. Analytical data suggest that they are present only in traces.

A corresponding observation was made using a two-dimensional arrangement instead of a solution in preparative amounts.[40] If a G4-SH monolayer on a silicon wafer is treated with small amounts of cluster solution, the particles quickly "disappear" in and underneath the monolayer. If the system is kept in an atmosphere of CH_2Cl_2, crystals appear in the course of a couple of days on the surface, where they can be imaged. Fig. 14 shows SEM images of such nanosized crystals in different magnifications. Though this procedure does not give sufficient amounts for further analyses, it can only be assumed that they are identical with the characterized crystals from solutions.

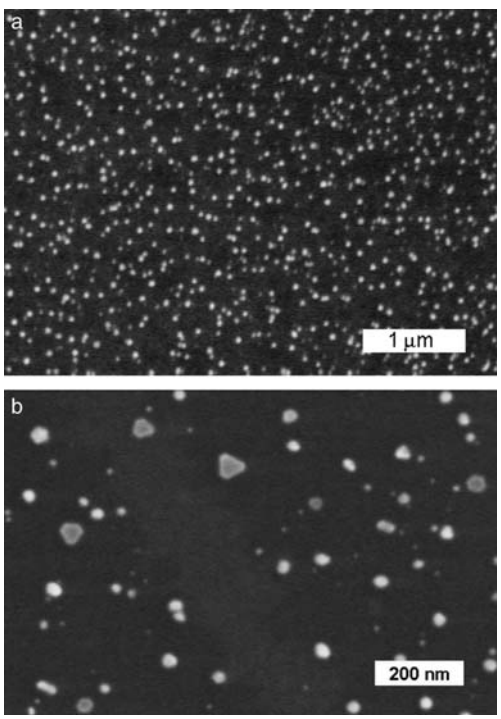

Fig. 14 SEM images of small crystals in different magnifications, generated in a monolayer of G4-SH from $Au_{55}(PPh_3)_{12}Cl_6$ in an atmosphere of CH_2Cl_2. (Reprinted with permission from ref. 40. Copyright 2005, Wiley-VCH).

2.4 The chemical resistivity of bare Au_{55} clusters

The indications of the thermodynamic stability of bare Au_{55} clusters, discussed above, provoked experiments with respect to their chemical behaviour.

Surface deposited bare Au_{55} clusters, separated from each other, were treated in an oxygen plasma. For comparison, the procedure was also applied to a series of smaller and larger non-full-shell clusters. After oxygen treatment, X-ray photoelectron spectroscopy (XPS) measurements where performed to analyse the presence of gold and gold oxides, respectively. Fig. 15 shows the result.[41]

As can be seen, the Au_{55} species only show a very weak oxidic shoulder, caused by few particles having a non-perfect full-shell cluster geometry. All other particles give well expressed signals for oxidic species. This result gives rise to study the catalytic properties of bare Au_{55} clusters, which should be of a special nature. However, experiments with Au_{55} have not yet been performed. Comparison with other naked gold particles in this respect would be of interest.[42]

A comparable result was obtained when the ligand-free clusters were treated with indium vapour. In bulk state, a

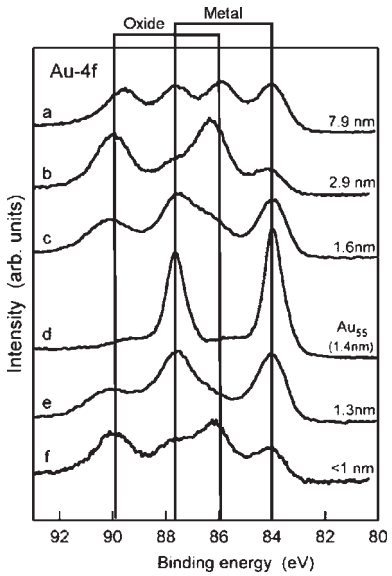

Fig. 15 Au-4f photoelectron spectra of different gold nanoparticles after treatment in an oxygen plasma. Only a very weak shoulder indicates some oxide from non-perfect particles. (Reprinted with permission from ref. 41. Copyright 2002, Science AAAS).

$AuIn_2$ phase exists which is easily formed from the elements. As in case of oxygen, all species used for comparison are at least partially alloyed if treated with In vapour, but not Au_{55}.[43]

The reason for the inertia of the Au_{55} clusters is to be seen in the perfect geometrical cuboctahedral shape. Any chemical reaction on the surface would require degradation of the full-shell system. Under the experimental conditions applied for the above experiments, the energy for a destruction of the particles is obviously not reached.

Finally, it can be stated that full-shell clusters are not only distinguished by a preferred formation, but even more by a special behaviour concerning the chance of survival. This can especially be followed from the tendency of ligand-free clusters to self-organize or to resist massive chemical treatment as discussed.

3. The special electronic behaviour of Au_{55}

A scientifically clear definition of nanoscience says that "nanoscience is dealing with functional systems either based on the sub-units with specific size-dependent properties or of individual or combined functionalized sub-units".[44] Considering metal nanoparticles, here it is the special case of the 1.4 nm particle Au_{55}, the relation to the definition is to be seen in the size-dependent properties. It is text book knowledge that a bulk metal is characterized by its freely mobile valence electrons, forming broad energy bands. On the contrary, in atoms or molecules, consisting of only a few metal atoms such as in $Co_2(CO)_8$, $Fe_3(CO)_{12}$ or $Co_4(CO)_{12}$, the electrons are located in discrete energy levels (atomic or molecular orbitals). A fundamental question therefore is where the transition from bulk to molecule happens if a metal particle is systematically reduced in size or, in other words, how many metal atoms are necessary to leave the typical molecular state. As it turned out by the study of numerous metal nanoclusters, $Au_{55}(PPh_3)_{12}Cl_6$ occupies exactly the position between bulk solids and molecules, at least at room temperature. At low temperatures, larger particles show similar behaviour since it is known that temperature drastically influences these critical electronic properties. It should also be recognized that any kind of electronic characteristics includes the presence of the ligand shell. The electronic properties of individual bare nanoparticles might be significantly different from those of ligand protected ones. A particle, indicating the existence of more or less concrete electronic energy levels can no longer be described using classical physical laws, rather quantum mechanical rules have to be applied (quantum dots) as is the case for atoms or molecules.

Some of the results indicating the quantum dot behaviour of ligand-protected Au_{55} clusters are summarized below. In some cases, comparison with other nanoparticles is suitable in order to indicate important differences. It should also be noted that the interest was mainly focused on room-temperature properties which should be of higher relevance for possible applications than low-temperature behaviour.

3.1 Answers from different tools

A valuable information on the electronic behaviour of Au_{55} in $Au_{55}(PPh_3)_{12}Cl_6$ came from the study of the *relaxation behaviour of excited electrons* in three different gold nanoparticles.[45] Using femtosecond laser spectroscopy, the relaxation time is found to be sensitive to the electron–phonon coupling as well as to the electron surface collision. In large particles, weakening of the electron–phonon coupling dominates and so slows down the electronic relaxation compared with bulk metals. The smaller the particles become, the more the surface collision dominates, accelerating relaxation. Fig. 16 informs on the relaxation behaviour of three differently sized gold nanoparticles.

As can be followed, the relaxation becomes faster going from 15 nm to 1.4 nm (Au_{55}) particles due to the increased surface collision. However, the still smaller 0.7 nm (Au_{13}) cluster exhibits drastically reduced relaxation. Whereas the relaxation of 15 nm and 1.4 nm is attributed to the formation of hot electrons (390 nm excitation), the molecular nature of the Au_{13} cluster is characterized by bonding electrons, fixed between the Au–Au bonds. In other words, these results characterize Au_{55} as a species, just one step before being a typical molecule. On the other hand, it behaves characteristically different from 15 nm particles, not to speak of the bulk metal.

This very special electronic situation of $Au_{55}(PPh_3)_{12}Cl_6$ is impressively confirmed by various other physical tools. The decisive difference between Au_{55} and colloidal gold, shown above, (1.4 nm *vs.* 15 nm) is also demonstrated by *optical spectroscopy*. In contrast to the well known collective dipole resonance (surface plasmon resonance) of larger gold nanoparticles at *ca.* 520 nm, responsible for the well known red colour of such particles, it can not be observed for extremely pure samples of $Au_{55}(PPh_3)_{12}Cl_6$.[46] Very small amounts of colloidal impurities result in weak plasmon bands. Consequently, this method can also be used to check the purity of Au_{55} cluster samples.

A more detailed view into Au_{55} clusters has been gained using *Mössbauer spectroscopy*. Mössbauer spectroscopy is a valuable tool to obtain information on the interaction of so-called Mössbauer nuclei and surrounding electrons. The electrical monopole-interaction is measured as the isomer shift δ (IS). It informs on the s electron density and so gives information on the oxidation state and coordination number. The electrical quadrupole interaction, measured as quadrupole splitting (QS), gives, among others, information on the ligand field splitting, again a very valuable information on the internal bonding situation in relevant compounds. Furthermore, information about the magnetic state of a system can be gained. For $Au_{55}(PPh_3)_{12}Cl_6$ the most valuable information comes from IS and QS. Table 1 summarizes the measured IS and QS data of the cluster and for comparison the corresponding data for bulk gold are added, together with a sketch of the bare Au_{55} nucleus, indicating the various types of Au atoms.[47]

The cuboctahedral $Au_{55}(PPh_3)_{12}Cl_6$ has five distinct Au sites: the central Au atom in the inner Au_{13} nucleus and its 12 surrounding atoms, 24 non-coordinated surface atoms, 6 Cl atoms located in the centres of the 6 squares and 12 corner surface atoms with coordinated PPh_3 ligands. The central Au atom and the 12 atoms in the first shell have the same nearest neighbour coordination and so do not differ visibly in IS and QS. However, the three sites in the second shell can well be

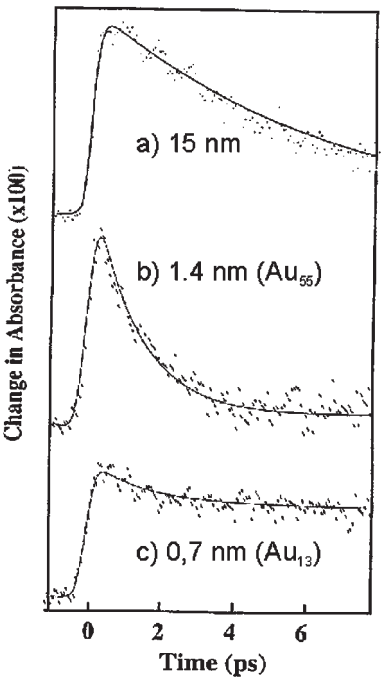

Fig. 16 The relaxation behaviour of excited electrons in three differently sized gold nanoparticles. (Reproduced with permission from ref. 45. Copyright 1997, Elsevier).

distinguished as can be seen from Table 1. Furthermore, it can be seen that the IS value of the central 13 atoms differ characteristically from the IS value of bulk gold. This difference is caused by the slightly lower s electron density in the Au_{13} core due to charge transfer to the ligands.

EXAFS studies on $Au_{55}(PPh_3)_{12}Cl_6$ at 80 K showed that the Au–Au bond lengths in the cluster are significantly shorter than in bulk gold and clearly indicate the cuboctahedral packing of the gold atoms, but not the existence of a polyicosahedral geometry.[48] Similar results were obtained for the water-soluble derivative $Au_{55}(Ph_2PC_6H_4SO_3Na)_{12}Cl_6$.

Table 1 Mössbauer spectroscopy data (IS and QS) of $Au_{55}(PPh_3)_{12}Cl_6$. The sketch of the Au_{55} core indicates the different types of surface atoms

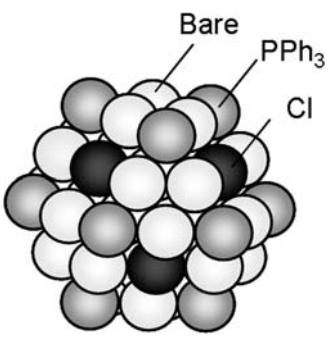

Au site	IS/mm s^{-1}	QS/mm s^{-1}
Core	−1.4	0.0
Bare surface	+0.3	1.4
PPh_3-bonded	+0.6	7.1
Cl-bonded	+0.1	4.4
Bulk gold	−1.224	0.0

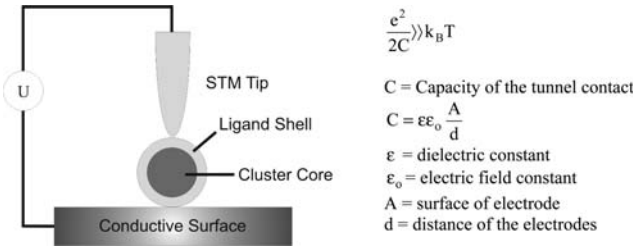

Fig. 17 Experimental setup to image and to investigate ligand protected nanoparticles by STM and STS, respectively. The conditions to observe single electron transitions are that $e^2/2C \gg k_BT$ where $C = \varepsilon\varepsilon_0 A/d$ is the capacity of the tunnel contact (ε = dielectric constant, ε_0 = electric field constant, A = surface of electrode, d = distance of the electrodes).

Corresponding investigations on the icosahedrally shaped $[Au_{11}(Ph_2PC_6H_4Cl)_7]I_3$ clearly show the difference in the typical nearest Au–Au distances linked with its icosahedral nature.

Finally, a last method shall be discussed completing our knowledge on the electronic situation in Au_{55} clusters in a unique manner: *scanning tunneling microscopy* (STM) and *spectroscopy* (STS). STM can be used to image individual cluster molecules, but of more valuable, to directly "look" into the electronic properties of quantum dots, is STS. The method is based on the electric contact between the STM tip and an individual particle, not a simple challenge. Using an experimental setup as sketched in Fig. 17, current (I)–voltage (U) characteristics can be obtained, telling us very valuable details about the particle's electronic behaviour.

The voltage U, applied between the STM tip and the conductive surface (a second STM tip can also be used instead), induces a current I, the value of which depends on the capacity C of the system. C is dependent on the tip distance d (in case of contact with the particle it is the thickness of the ligand shell), the surface of the electrode and the particle size, respectively, as well as of the dielectric constant ε and the electric field constant ε_0. In other words the smaller the particle, the smaller is C. In the case of a quantum dot between the electrodes, single electron transition should be observable, assuming that either the thermal energy of the electrons or C is small enough so that the condition $e^2/2C \gg k_BT$ (k_B = Boltzmann constant) is fulfilled. An example how the temperature influences the situation is impressively shown when a 17-nm Pd particle, protected by a shell of $H_2NC_6H_4SO_3Na$ ligand molecules and trapped between two platinum electrodes, is investigated at two different temperatures.[49] The result, shown in Fig. 18, clearly demonstrates that the nanoparticle behaves in bulk-like manner at 295 K, following Ohm's law, but shows a well expressed step, the so-called Coulomb blockade (CB), at 4.2 K.

The CB behavior tells us that there exists a gap voltage of *ca.* 55 mV where a single electron is trapped in the particle and is only released at higher voltage. This behaviour indicates the existence of a single electron switch at 4.2 K. The question, already asked at the beginning of this chapter, namely how small a metal particle has to be in order to reach typical quantum dot behaviour at room temperature, has been

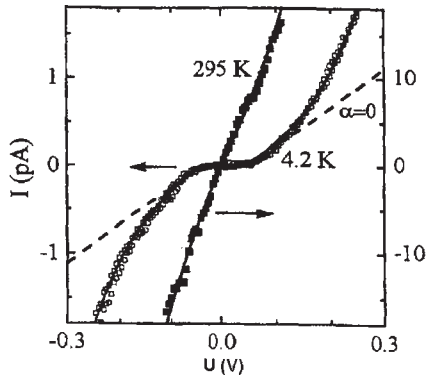

Fig. 18 Current (I)–voltage (U) characteristics of a 17-nm Pd particle at 295 and 4.2 K. (Reprinted with permission from ref. 49. Copyright 1997, American Institute of Physics).

studied with particles of different size. As has been found, even the four-shell cluster $Pt_{309}(phen^*)_{36}O_{30}$ (phen* = sulfonated phenanthroline) with its 1.8 nm Pt core shows a Coulomb blockade only at low temperatures, not at room temperature.[50]

The unique situation of Au_{55}, already variously mentioned, again becomes visible by STS. Individual $Au_{55}(PPh_3)_{12}Cl_6$ clusters, deposited on a gold substrate, show indeed a Coulomb blockade at room temperature (!), as is seen from Fig. 19.[51]

Due to a sufficiently small C value, $e^2/2C$ is large enough to fulfil the above condition. This is the first example of a single electron switch working at room temperature! Of course, this finding gives rise for thinking about future applications of these quantum dots in nanoelectronic devices, as will be discussed in section 3.2.

An even deeper insight into the electronic situation of $Au_{55}(PPh_3)_{12}Cl_6$ is gained if STS is applied at low temperature. Investigation at 7 K in a low-temperature ultrahigh vacuum scanning tunnelling microscope resulted not only in individual images (Fig. 20) of the nanoclusters, but gave very valuable information on the electronic level splitting in the Au_{55} nucleus.[52,53]

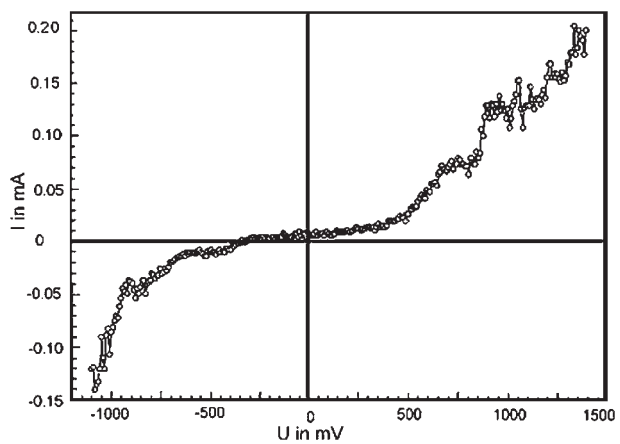

Fig. 19 I–U characteristic of $Au_{55}(PPh_3)_{12}Cl_6$ at room temperature indicating a well expressed Coulomb blockade. (Reprinted with permission from ref. 51. Copyright 1998, Springer).

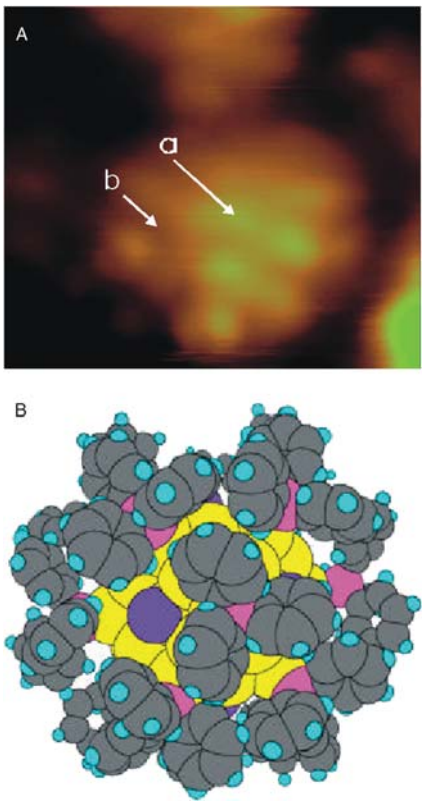

Fig. 20 Left: STM image of a single $Au_{55}(PPh_3)_{12}Cl_6$ cluster. The light green areas represent electron rich phenyl rings of the PPh_3 ligands. The positions a and b have been used to measure STS spectra (see Fig. 21). Right: model of the cluster of the corresponding view. (Reprinted with permission from ref. 53. Copyright 2003, American Chemical Society).

Fig. 20 shows an STM image of $Au_{55}(PPh_3)_{12}Cl_6$ and the corresponding model. The light green areas indicate the position of electron-rich phenyl rings of PPh_3. The positions a and b indicate where the spectroscopy has been performed. In order to exclude any influence of the ligand molecules on the result, measurements were performed over a Ph ring (a) and, in the same distance, over a ligand-free position (b). As could be expected, clear Coulomb blockades of the same extension could be observed in both cases. Due to the low temperature, the blockade is extended compared with the 295 K measurement, to be followed from Fig. 21. If the I–U characteristic is changed in such a way that the first ablation dI/dU is used instead of I, CB is indicated as a minimum. Due to the low temperature of 7 K, this minimum is now characterized by a series of energy levels with average spacing of 170 meV. This result clearly proves the disappearing of the energy bands, present in the bulk state to the replacement by discrete levels, as is in principle the case in atoms. Quantum dots therefore are often called ''artificial big atoms''.

After having characterized and discussed the specific electronic properties of individual cluster species, it is of interest how ligand protected Au_{55} clusters interact electronically with each other under varying conditions. Very first results have been gained by using impedance spectroscopy to investigate macroscopic pellets of $Au_{55}(PPh_3)_{12}Cl_6$ of high density (91% of the theoretical density) with respect to the electronic inter-cluster

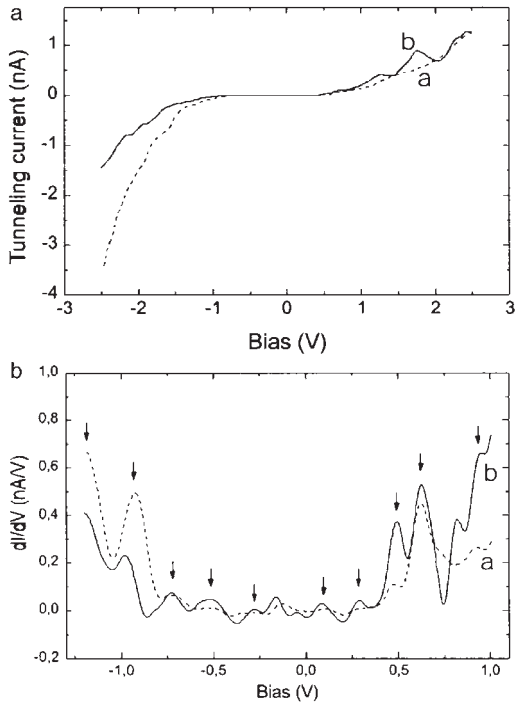

Fig. 21 Left: I–U characteristics of a single $Au_{55}(PPh_3)_{12}Cl_6$ cluster at 7 K measured at two different positions (see Fig. 20). Right: dI/dV characteristic of the curves a and b indicating discrete energy levels with spacing of 170 mV. (Reprinted with permission from ref. 53. Copyright 2003, American Chemical Society).

relation.[54–56] The experimental results, obtained at temperatures between 253 and 333 K, indicate that in the borderline region from bulk to molecule the last "metallic" valence electrons are localized in a quantum box of the lateral dimension of the cluster, wherein they are freely mobile at the applied temperatures. Corresponding to the Pauli principle, the quantum box in $Au_{55}(PPh_3)_{12}Cl_6$ is occupied with two electrons. If a third electron enters, the cluster core serves as an electron trap. The inter-cluster conductivity is determined by the tunnelling of single electrons. An activation step and transport step result in the tunnelling step which corresponds to a disproportionation step resulting in the activation enthalpy. The relaxation frequencies are in the region of 10^4–10^5 Hz. The total resistance at 298 K is found to be 3.23×10^{-4} ohm^{-1} m^{-1} and the temperature dependence of the dc and ac conductivity follow the Arrhenius relation $\sigma(T) = \sigma_0 + \exp(-E_A/k_BT)$ (E_A = activation energy, k_BT = thermal energy). This relation indicates hopping transport of individual charges between nearest neighbours. At low temperatures, the number of charge carriers of the hopping process does not change with temperature. However, at elevated temperatures, thermally excited additional charge carriers participate in the hopping process. E_A reflects the energy necessary for the transport of an electron from one cluster to another.

Since at room temperature nearest hopping dominates, it was of interest to vary the cluster–cluster distance by thicker ligand shells or by spacer molecules of different lengths. Generally, two types of distance separators are possible: those linking the clusters covalently and those linking them non-covalently, for instance by simply touching one another or by ionic interactions. The sketch shown in Fig. 22 shows the various kinds of distance separators between identically sized Au_{55} nuclei.[57]

For type I the standard PPh_3 and T_8-OSS-SH ligands (see Fig. 3), enlarging the total diameter of the cluster from 2.2 nm to about 4.2 nm, have been applied. Diamines are used to link the clusters *via* ionic bonds using the acidic ligand

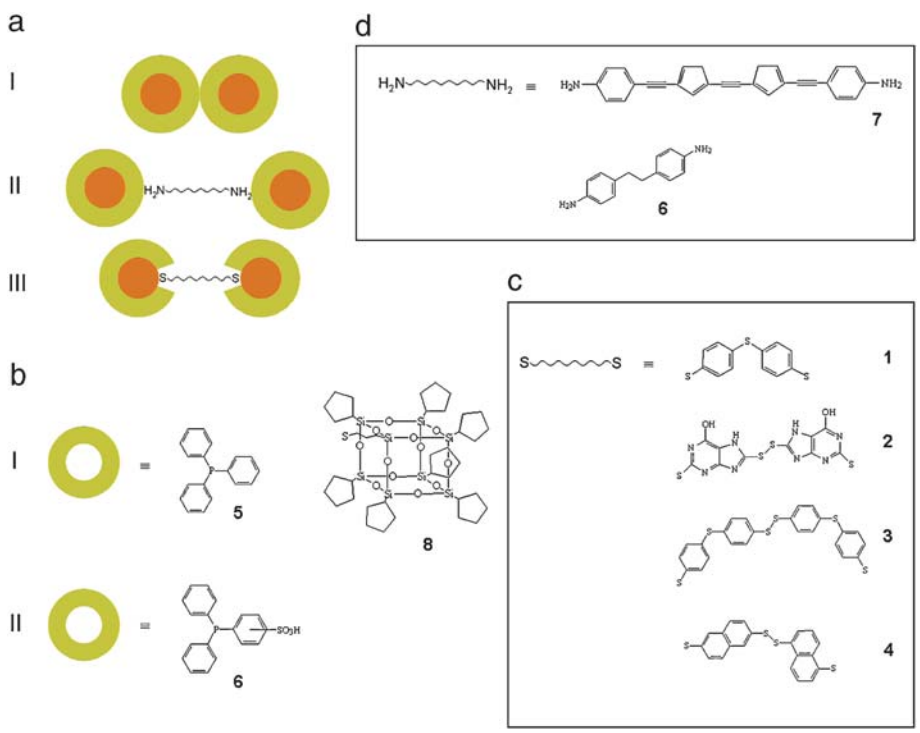

Fig. 22 Principles of variations of cluster–cluster distance.

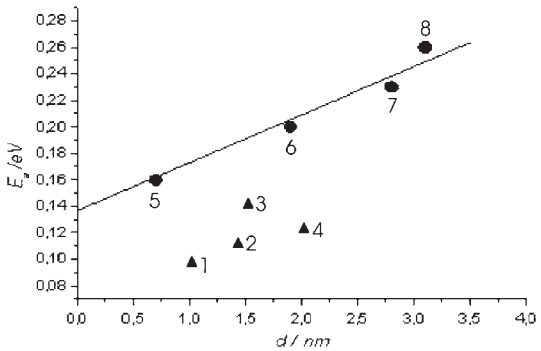

Fig. 23 Activation energies of variously linked Au_{55} clusters. Covalently linked clusters (**1–4**) show characteristically reduced E_a values compared with non-covalently linked species (**5–8**).

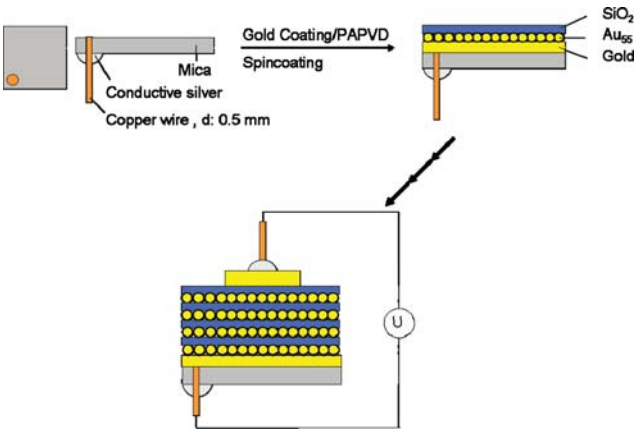

Fig. 24 Sketch of the construction of electrically contacted cluster/SiO_2 multilayers.

$Ph_2PC_6H_4SO_3H$ (type II), and covalent cluster–cluster bonds were obtained by dithiol molecules, each S atom substituting a PPh_3 ligand (type III). Without going into chemical details, Fig. 23 informs on the measured activation energies as a function of the different distances.

The activation energy increases linearly for the non-covalently linked clusters with increasing distance (**5–8**). The covalently communicating systems **1–4** show significantly lower activation energies, due to the better conductivity of the molecules used, all consisting of conjugated π-systems.

The investigation of charge transport in three-dimensionally organized Au_{55} clusters has been extended to the study of two-dimensional cluster arrangements. However, as it turned out, the resistance of larger monolayers is too high to be measured. Only small areas of about 20 nm show sufficient conductivity to be determined. Such 20 nm areas of $Au_{55}(PPh_3)_{12}Cl_6$ result in *I–U* characteristics with well expressed Coulomb blockades like in the case of single clusters.[58] However, *I–U* and impedance measurements on $Au_{55}(PPh_3)_{12}Cl_6$ multilayers succeeded if measured in a vertical direction.[57,59,60] Multilayers are made by using self-assembled monolayers of thiol molecules on flat substrates. These bind the clusters by partial substitution of PPh_3 by thiol functions. Additional deposition of a thiol monolayer on the cluster monolayer then allows the generation of a third cluster monolayer *etc*. The as prepared 300–500 nm thick films were characterized by TEM and AFM. The electrical response, measured parallel to the surface, resulted in thermally activated conductivities, similar to that observed for 3D systems (see above).

A very different type of cluster multilayers has been generated and investigated.[61,62] The conductivity behaviour of $Au_{55}(PPh_3)_{12}Cl_6$ double- and monolayers, embedded between 5 nm SiO_2 films, was measured perpendicular to the film plane. The SiO_2 films were generated by a plasma-assisted physical vapour deposition (PAPVD) and the cluster films by a spin-coating process. AFM and scanning electron microscopy (SEM) characterization of the layer systems were used for quality control. Fig. 24 shows a sketch showing the generation procedure, Fig. 25 shows TEM images of cluster/SiO_2 multilayer samples.

Impedance measurements of the cluster double layer systems <15 nm indicate thermally activated frequency dependence of the capacitance. It is assumed that in the cluster double layers dipoles are formed which then interact between the layers at low frequencies. Multilayer systems >15 nm tend to crystallize.[61]

The multilayer systems containing cluster monolayers behave characteristically different.[62] Samples of up to eight cluster/SiO_2 combinations have been investigated. Current–voltage relation studies between -5 and $+5$ meV show linear *I–U* characteristics. This is interpreted as the result of electron tunnelling from the cluster monolayers through the SiO_2 films or, in other words, the cluster monolayers are in contact with each other through the SiO_2 films. The current values decrease with increasing number of layers. From the linear *I–U* characteristics it can be followed that there is no tunnelling

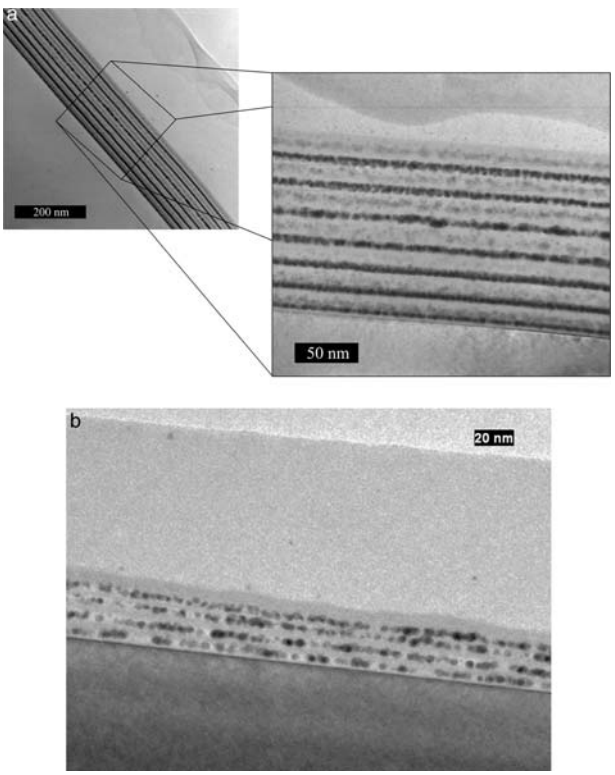

Fig. 25 SEM images of cluster double layers (a) and monolayers (b), separated by SiO_2 films. (Reprinted with permission from ref. 61 and 62. Copyright 2005, Wiley-VCH).

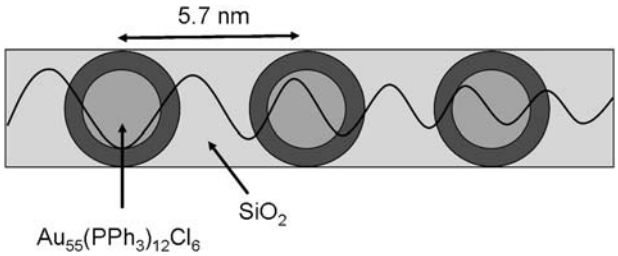

Fig. 26 Illustration of electronic tunnelling through cluster/SiO_2 layers with decreasing amplitude.

blockade. The tunnelling distance is about 5.7 nm. Fig. 26 illustrates the electronic situation in such a system.

The amplitude of the electronic wave is found to decrease with an increase in the number of layers.

It seems important to keep in mind that there is a characteristic difference between the systems with cluster double layers and those with monolayers. Thus dipoles are formed in the double layers, which is not possible in monolayers, so that tunnelling processes dominate in monolayers.

Finally, a very special electric behaviour of a $Au_{55}(PPh_3)_{12}Cl_6$ monolayer shall briefly be discussed. A cluster monolayer was generated on a thin film of PVP (see 2.2.2), deposited on a SiO_2 support and contacted by two electrodes.[63]

Fig. 27 shows an SEM image of the experimental setup.

Like in former experiments (see above), the resistance of the monolayer was too high to be measured. However, for obtaining the above SEM image, the sample was irradiated with a 10 keV electron beam for 10 s with the consequence of a measurable current of roughly Ohmic behaviour. However, if only one electrode and part of the monolayer is irradiated, a diode-like characteristic can be observed, as can be followed from Fig. 28(a).

The diode behaviour can be tuned by variation of the energy of the electron beam, the exposure time, the contact distance and the irradiated area. Optimum conditions are 10–20 keV, 10 s and an electrode distance of 50 nm. A second surprise is the fact that the system relaxes in the course of 15–30 h after

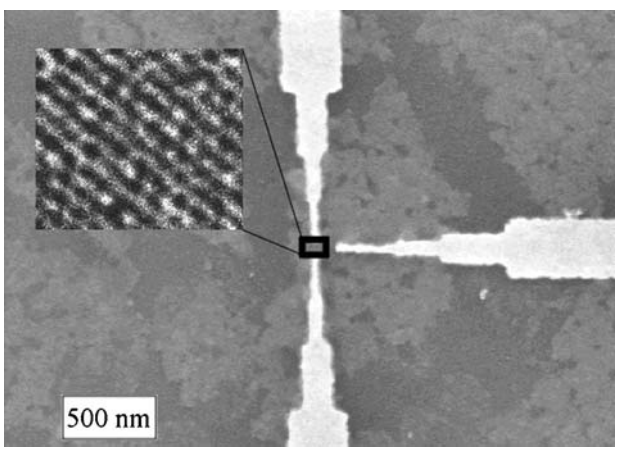

Fig. 27 SEM image of the experimental setup for measuring the conductivity behaviour of a cluster monolayer on PVP using a SiO_2 support. (Reprinted with permission from ref. 63. Copyright 2001, Wiley-VCH).

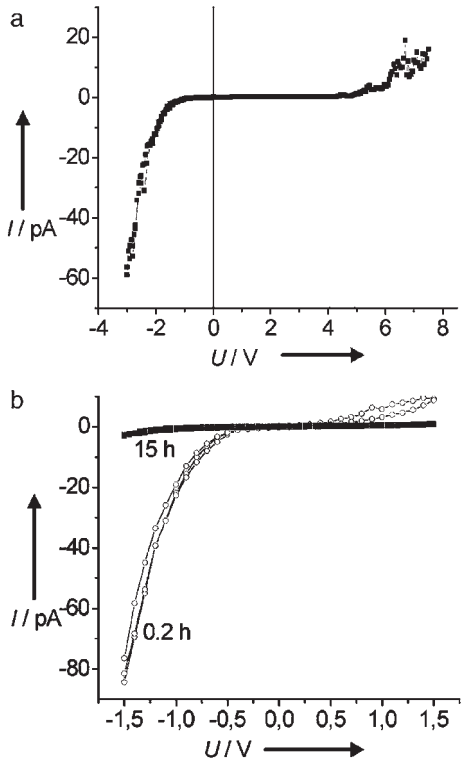

Fig. 28 (a) Diode behaviour if one electrode and part of the monolayer are irradiated by an electron beam. (b) Relaxation of the diode situation in the course of 15 h. (Reprinted with permission from ref. 63. Copyright 2001, Wiley-VCH).

switching off the voltage, as is seen from Fig. 28(b). Reactivation is possible in any case *i.e.*, there is no degradation or decomposition during irradiation. An explanation for this very unusual observation is that so-called "image charges" in the cluster layer are formed as a consequence of additional charges in the SiO_2 surface. Due to this activation process, the particles reorganize in the layer in order to reach maximum distance and minimum energy, for instance square instead of hexagonal. This process happens rapidly during the electron bombardment but takes much more time to reorganize after switching off the voltage.

All these experimental results, beginning with the quantum dot behaviour of individual Au_{55} clusters up to the electronic interactions in three- and two-dimensional arrays indicate the exceptional position of ligand protected Au_{55} nanoclusters. Based on these fundamental investigations it is obvious to conjecture about possible applications of Au_{55} clusters. Some of the activities, even if still very underdeveloped, are discussed in the following section.

3.2 Possible applications

Among the numerous exciting properties of $Au_{55}(PPh_3)_{12}Cl_6$ and its derivatives, the ability to be switched by single electrons is probably the most promising one, considering future applications. There is an ultimate vision, namely to use these quantum dots as switches and transistors in nanoelectronic memory systems and computers, especially since the well-known Moore law predicts the need of novel generations of transistors in the

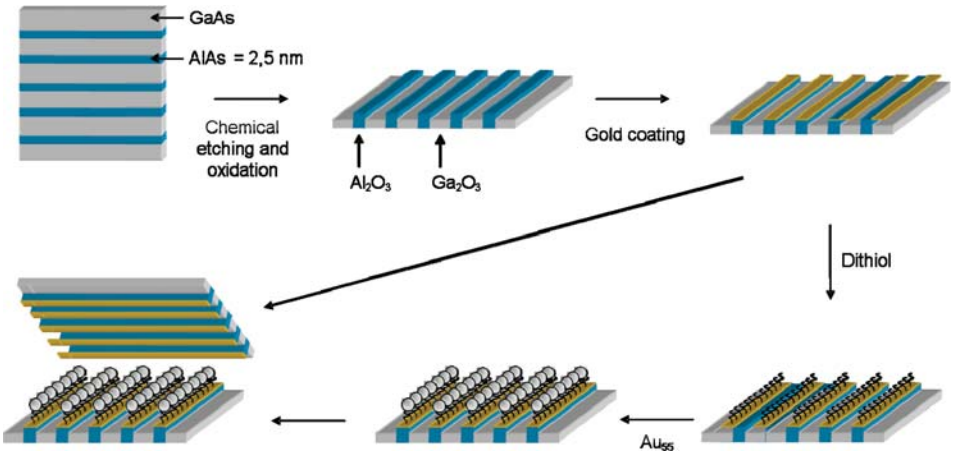

Fig. 29 Sketch of the aimed construction of a cross-bar system with single quantum dots between each cross-point.

next few decades.[64] Another reason to think about the use of single electron transistors is the fact that at present transistors use some hundred thousands of electrons for each 0/1 step. Au_{55} could do it with one single electron, an enormous reduction of energy. However, the step from the individual particle to a working system is accompanied by any number of technical difficulties and it may be that some of them can never be solved. In spite of the huge challenges to be foreseen, it seems worth to start at least with some very first steps on the way to the goal, the realization of which would open the door to absolutely novel generations of computers. A change from the present transistor size in modern computers to 1.4 nm quantum dots would increase the storage capacity by at least a factor of thousand. Therefore, any kind of effort seems justified.

The most difficult challenge is to be seen in the connection of the nanosized switches and transistors among one another and to the macroscopic outer world, respectively. The first step is the generation of an aimed arrangement of quantum dots on atomically flat surfaces, including electrical contacts. To begin with, it seems reasonable to find solutions for arranging and contacting the clusters by using them only as switches and not yet as transistors. A cross-bar system, consisting of conducting wires of appropriate diameter, having a switch between each cross-point, would allow to electrically address each of the quantum dots. Fig. 29 shows a sketch of the planned arrangement.

Conductive bars of 2.5 nm in diameter would be ideal for arranging the $Au_{55}(PPh_3)_{12}Cl_6$ clusters strictly one-dimensionally. However, to get a first experience, groups of parallel 20 nm wide bars were generated, beginning with a multilayer system of epitaxially grown alternating GaAs and AlAs layers.[65]

Part of the multilayer system is first oxidized by H_2O_2, followed by an etching process with citric acid and repeated oxidation. The successful generation of this Al_2O_3 bar system is demonstrated by AFM and SEM (Fig. 30).

Shadow mask evaporation of gold finally gives conductive bars that can be decorated with Au_{55} clusters *via* 1,4-benezendithiol. This process is in principle known from former experiments with two-dimensional extension. Due to the bar dimension, a maximum of 8–9 clusters might be arranged in parallel on the gold traces. The presence of the clusters has been shown by electrical measurements before and after the decoration. The cluster protected bars show a drastically increased resistivity.

Finally it could be demonstrated that also 2.5 nm Al_2O_3 bars can be generated, using the same technique, as is shown in Fig. 31.[65]

Deposition of gold and clusters on the 2.5 nm bars has not yet been demonstrated. Furthermore, it has also not yet been shown that addition of a gold wire system perpendicular to the first one indeed results in a successful contact of clusters between each at the cross-points. On the other hand, the experiments described above give hope for a successful further development.

4. Biological responses to gold nanoparticles

The interaction of nanoparticles in the size range of 1–100 nm with biological systems is of general interest for several

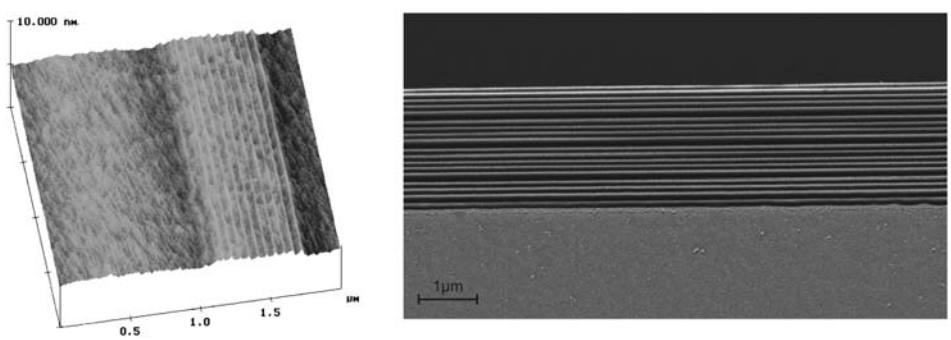

Fig. 30 AFM (left) and SEM image of bundles of 20 nm Al_2O_3 bars.

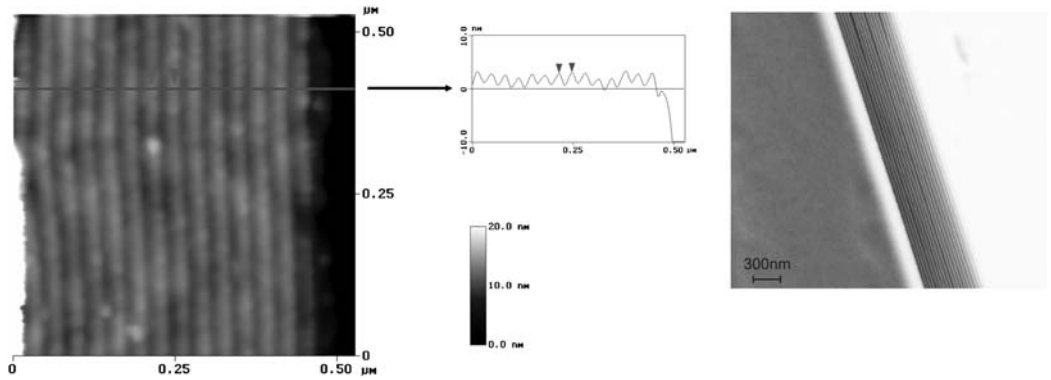

Fig. 31 AFM (left) and SEM image of bundles of 2.5 nm Al_2O_3 bars.

reasons. One is the similarity of the particle size and that of cellular components and proteins. Gold nanoparticles of various size and shape have frequently been in the focus of interest. Another reason for the use of gold nanoparticles is the fact that they can easily be identified by electron microscopy and/or by UV-Vis spectroscopy if not too small. Furthermore, the noble character of gold restricts the variety of interactions with biomolecules. Oxygen sensitive particles like those of iron, cobalt *etc*. would immediately be oxidised in aqueous media under *in vivo* conditions and so would no longer behave as the original particles. Such metal nanoparticles may also dissociate ions from the surface and so cause additional chemical reactions.

As will be shown later, the ability for interactions depends decisively on the particle size. Numerous papers in the recent past report on the toxicity or otherwise of gold nanoparticles. These findings can not be considered absolutely, but must be judged in dependence of the particle size. In addition, other as important factors influencing the behaviour of gold nanoparticles in a living medium exist. Most decisive is the nature of the particle's surface. Since bare particles do not exist at all under usual experimental conditions, the particles have to be equipped by a shell of ligand molecules. These protecting compounds, whatever they may consist of, make the very first contact to molecules in a new medium and influence transport mechanisms as well as the metabolic behaviour. In addition, electric charges may be located on the surface. Positively or negatively charged surfaces may behave very different, even if the chemical composition of the ligand material might be comparable. Considerations like these are of general nature and originate from our basic knowledge of complexation chemistry. In this sense, interactions of metal nanoparticles with biomolecules, even if very complex, are related to complex chemistry, and are often difficult to understand and to observe. Nevertheless, it is complex chemistry and from this we know that the stability of a complex depends on the bond strength between the metal atom and ligand molecule, its geometry and extension which additionally influences the stability of a complex. Strong ligands substitute weaker ligands, an important fact also in biosystems. Furthermore, the complex stability depends on the number of functionalities in a ligand molecule. A bi-, tri-, tetra- or even oligodentate ligand forms complexes the stability of which exceeds that of complexes with chemically equivalent monodentate ligand molecules by orders of magnitude. The stability constant of a complex informs on these relationships.

Having all these manifold and in some cases rather difficult relations in mind, an absolute statement on toxicity or non-toxicity of gold nanoparticles is not possible. Each example has to be considered independently with consideration of the respective situation. In the following, some examples from the recent literature are briefly and critically discussed on condition of the above statements.

4.1 Toxicity and non-toxicity of gold nanoparticles

4 nm gold particles, protected with cysteine or citrate, 12 nm particles, generated by reduction with glucose, and 18 nm particles, alternatively modified with citrate, biotin and cetyltrimethylammonium bromide, have been used to interact with human leukemia cell lines (K562).[66] Though the particles have been taken up into the cells, no inherent toxicity has been observed. Except for citrate, which was present on the 4 nm and on the 18 nm particles, all other test compounds had very different surfaces. There is a dramatic difference between citrate and cysteine. Citrate anions are only weakly coordinated to the gold surface and can easily be substituted by almost any other molecule, whereas cysteine forms stable Au–S bonds. Independent on the fact that both species do not show toxicity, it can be expected that they behave very differently in contact with the cell lines. Glucose or its oxidation products on the 12 nm species, biotin and cetyltrimethylammonium-cations, equip the 18 nm particles with fundamentally different surface properties, so that the reasons for the non-toxicity of the particles can be seen in the size of the particles and/or in the ligand shells. The conclusion of these investigations is only that each individual species exhibits no toxicity towards leukemia cells, specific reasons can not be given.

The uptake of spherical and rod-shaped gold nanoparticles in the size range of 10–100 nm by HeLa cells, fully or at least partially (rod-shaped) modified by citric acid ligands, has been studied.[67] It could be shown that the kinetics and saturation concentrations depend characteristically on the dimension of the particles. A maximum uptake was observed for 50 nm particles. It is assumed that the uptake of the nanoparticles is mediated by non-specific adsorption of the particles on serum proteins. These results are consistent in so far as the particles of different size and shape all have predominantly the same kind of surface, so that different behaviour can indeed be

traced back to the particles size and shape. Transferrin equipped gold nanoparticles exhibited the same trend in uptake, but with a reduced level. In agreement with the results described in ref. 66, no cellular toxicity could be observed.

The response of macrophages (RAW264.7) to gold nanoparticles has also been investigated recently.[68] 35 ± 7 nm gold particles, capped by lysine and poly-lysine, were studied with respect to endocytotic uptake and cell toxicity. As in the cases discussed above, cytotoxicity could not be registered. Instead, a production of reactive oxygen and nitride species was observed.

Peptide modified gold nanoparticles were used to investigate subcellular distribution in HeLa human cervical epithelium cells, in murine fibroblastoma (3T3/NIH) cells and in HepG2 human hepatocarcinoma cells.[69] Commercially available 20 nm gold particles were modified by four different peptides, conjugated to bovine serum albumin. It turned out that the kind of peptide used for the decoration determines the behaviour of the particles towards the cells. Location of the particles exclusively in cytoplasm, in cytoplasm and nucleus, and no uptake were all observed. A detailed discussion of these interesting results shall not be given due to the fact that obviously the biochemical nature of the particles surface and the cell type determine the trajectories, and not the gold particles in the centre, which was of same size in any case. Statements on toxicity are not given, but obviously it has not been observed.

Citrate covered 13.1 ± 1.4 nm gold particles were used to study the influence on human dermal fibroblast cells from primary cultures.[70] An easy transport through the cell membranes was observed with particle concentration in the vacuoles. As a consequence, abnormal actin filaments as well as formation of extracellular matrix species have been found.

Marked toxicity has been observed using 2 nm gold particles decorated with two different species, alkylammonium- and alkylcarboxylic-thiols, which are strongly bound to the particles surfaces *via* sulfur. The ammonium functions cause a positively charged surface, the carboxylic groups make the surface negative.[71] Red blood cells, Cos-1 cells and *E. coli* bacteria have been selected for toxicity tests. As it turned out, the anionic species showed no toxicity at all, whereas the positively charged species indicate a moderate toxicity with respect to the selected cells and bacteria, respectively. Again, it is the particle's surface that determines the toxicity or non-toxicity, and not so much the size of the particle.

Summarizing these investigations of bio-responses on various gold nanoparticles it can be stated that in most cases the nature of the surface is responsible for the nature of interaction with the cell lines under investigation. A direct dependence of toxicity from the particle size has not yet been shown. Only in one case it could be observed that for citrate modified particles, a maximum uptake for 50 nm particles happened, but without the consequence of toxicity. Furthermore, it was not expressively documented that the protecting materials are toxic or non-toxic by themselves to see if the additional presence of gold particles plays any significant role. In other words, up to now there has been no clear proof of toxicity of gold nanoparticles at all, nor that in the case of toxicity is there a direct correlation between size and toxicity. In the following sections we present first results of a systematic investigation of the toxicity/size relation for gold nanoparticles.

4.2 The special size- and element-related responses to Au_{55}

Bulk gold is known to be non-toxic. Therefore, it has been applied in medicine, especially in dentistry, without any detrimental effects; even in colloidal form it has been used against rheumatic diseases. The question is however, what gold nanoparticles really do on a size level where intense interactions with cell components become possible on a molecular level. Another important question is the role of the element gold itself. Though gold is the most noble metal, it is also the most electronegative metal we know, comparable with iodine. Is therefore a special attraction between gold nanoparticles and negatively charged biomolecules to be expected? To get answers, we must find a way to directly interact gold nanoparticles with cell components, independent of the presence of a protecting core shell. The following sections will give some very first answers on these fundamental questions.

4.2.1 Au_{55}/DNA interactions. DNA, the most fascinating and fate determining part of a cell, is nowadays an available molecule either from natural cells or as artificial pieces of predetermined composition and length. Before beginning with studies of Au_{55} clusters in living cells, we investigated Au_{55}/DNA interactions *in vitro*. Natural DNA was used to interact with the water-soluble $Au_{55}(Ph_2PC_6H_4SO_3H)_{12}Cl_6$.[72] The interaction of metal nanoparticles with DNA is in general a well known phenomenon, and it is observed that nanoparticles usually organize along the DNA double strands by electrostatic interactions, among others observable by TEM. Au_{55} clusters behave decisively differently.

From preliminary AFM investigations it could be shown that the above cluster indeed adds to DNA in aqueous solution. Fig. 32 shows an AFM image of a y-formed piece of DNA with only partial cluster coverage.

As can be followed from the cross section through a non-covered and a covered part of the DNA, the difference between both is about 1.8 nm, less than the diameter of the ligand protected cluster. So, a simple addition of ligand protected clusters to the DNA surface could not have happened. Detailed TEM studies and molecular modelling calculations indicated what has actually occurred.

From numerous TEM investigations it is known that imaging of Au_{55} particles is in general no problem at all. However, TEM studies on systems, equivalently prepared to that shown in Fig. 32, resulted in the presence of parallel wires, consisting of particles of only 0.7 nm in diameter instead of 1.4 nm and additional larger gold particles of 5–10 nm, as can be seen from Fig. 33.

What happened? From molecular modelling calculations[72] we learned that there should exist an interaction between bare Au_{55} clusters and the major grooves of the B-DNA, existing under the experimental conditions in aqueous media. Two reasons for this very special interaction became obvious: first, a more or less perfect fit of about 50% of the clusters in the major grooves, the height of which is known from X-ray diffraction data and second, the electronegativity of gold, resulting in strong interactions between the negatively charged phosphates of the DNA and the particle surface. Fig. 34 shows the result of the calculations.

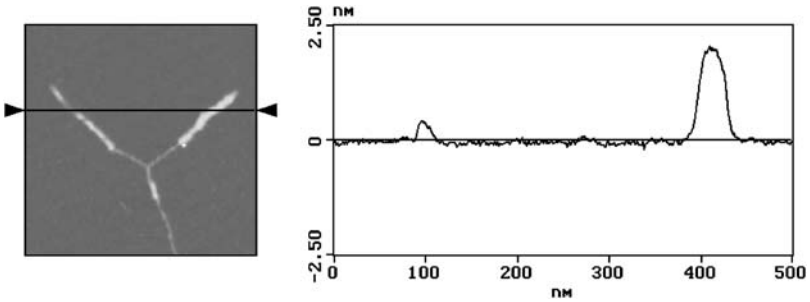

Fig. 32 AFM image of a y-formed piece of B-DNA, partially covered with clusters. The cross section shows the difference in height between non-covered and covered DNA (*ca.* 1.8 nm). (Reprinted with permission from ref. 72. Copyright 2003, Wiley-VCH.)

Chemically, the formation of these hybrid systems can well be understood: it is the substitution of rather weakly coordinated monodentate phosphine ligands by multidentate negatively charged groove entities, enveloping the clusters by about half of their volume. It can not be determined if residual phosphines are still located on the outside.

Why is this arrangement not to be seen in the TEM and why do we find 0.7 nm particles, instead? The answer is to be seen in the transformation of the B-DNA into A-DNA under the ultra-high vacuum conditions in the electron microscope. These lead to the loss of water from B-DNA, linked with a shrinking and reduction of the dehydrated major groove height from *ca.* 1.5 nm to 0.7 nm.[73] One might have been expected that the shrinking process is avoided due to the presence of the 1.4 nm gold spheres or alternatively, the elimination of the clusters might occur. Instead, the 1.4 nm spheres are degraded to the fitting 0.7 nm clusters (corresponding to Au_{13}) which now form as stable complexes with the water-free A-DNA. The gold atoms, peeled of from the Au_{55} clusters, aggregate to larger nanoparticles which can be found everywhere in the sample, and two of them can be seen in Fig. 33(a). Molecular modelling calculations of the interaction of idealized Au_{13} clusters with A-DNA resulted in the situation shown in Fig. 35. Inter-strand interactions lead to the wire-like structure to be seen in TEM.

These results impressively show the exceptionally strong interaction of fitting gold nanoparticles with the major groves of B- and A-DNA, respectively. The results also demonstrate that Au_{55} clusters, if available as bare spheres, could irreversibly attack DNA in living cells, if no other strong interactions on the way through the cell membranes and the inner cell parts prevent arrival in the nucleus. Again, it should be reminded that a metal atom (here it is a very small nanoparticle) in a mixture of weaker and stronger ligands finally ends up complexing with the strongest of them. To see if DNA is the

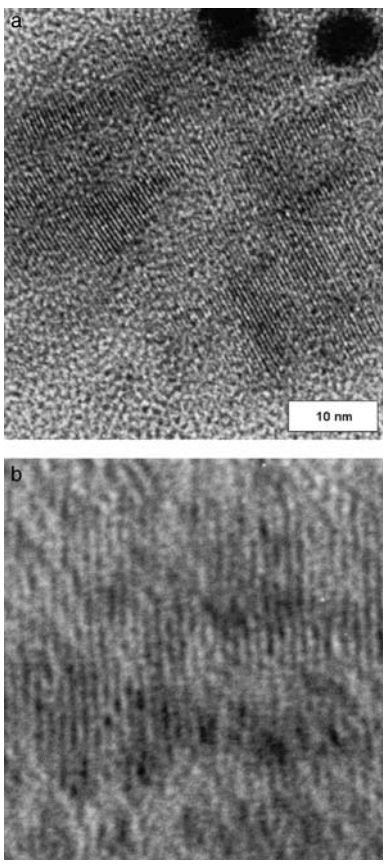

Fig. 33 TEM image of 0.7 nm gold particles organized in parallel wires and large gold nanoparticles (a) and a magnified cutout (b), generated from DNA/Au_{55} interaction and ultra-high vacuum conditions. (Reprinted with permission from ref. 72. Copyright 2003, Wiley-VCH.).

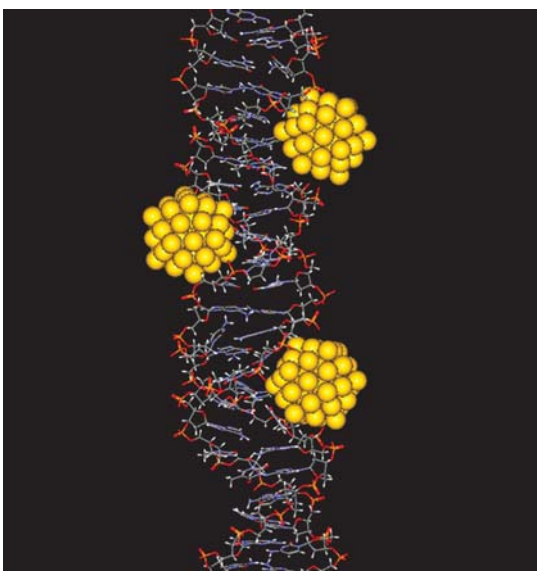

Fig. 34 Modelling of the interaction of bare Au_{55} clusters with the major grooves of B-DNA. (Reprinted with permission from ref. 72. Copyright 2003, Wiley-VCH.).

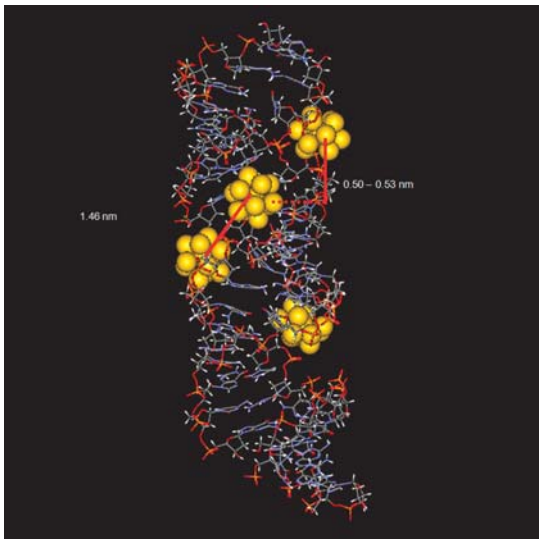

Fig. 35 Molecular modelling of Au_{13} clusters in A-DNA. (Reprinted with permission from ref. 72. Copyright 2003, Wiley-VCH.).

ultimate partner for Au_{55} in a complex cell system, offering numerous other potential reaction partners, the cell experiments described in the next section have been performed.

4.2.2 Au_{55}/tumor cell interactions. A series of human cancer cell lines has been selected to study not only the cytotoxicity, but also to observe the distribution of the gold clusters in the various cell compartments. Parallel experiments have been carried out with the routinely applied chemotherapeutical cisplatin.[74] First of all, a possible toxicity of the ligand molecule $Ph_2PC_6H_4SO_3H$ and its Na-salt has been investigated. As it turned out, there is no difference to be observed if the SO_3H or the SO_3Na derivative is used, and both are non-toxic. Table 2 presents the cell lines selected for the tests and the IC_{50} values for cisplatin and the Au_{55} cluster. IC_{50} is defined as the concentration of drug required to inhibit cell growth by 50% compared to a control. It should be mentioned that the incubation time for cisplatin was 74 h compared with only 24 h for Au_{55} in order to get comparable results.

Comparable IC_{50} values can only be registered for SK-ES1, MOR/P and CCD-919 Sk, neglecting the factor 3 in time. All other data indicate a dramatically higher cytotoxicity of the Au_{55} clusters compared with cisplatin. The maximum difference is observed for the metastatic melanoma cell-lines BLM and MV3 with a ratio of the IC_{50} values of *ca.* 180 : 1 for BLM and still far over that value for MV3. In fact, the difference of both compounds is still more significant since the Au_{55}-values have been reached already after 24 h. After 74 h, IC_{50} values could not be determined due to total mortality of the cells.

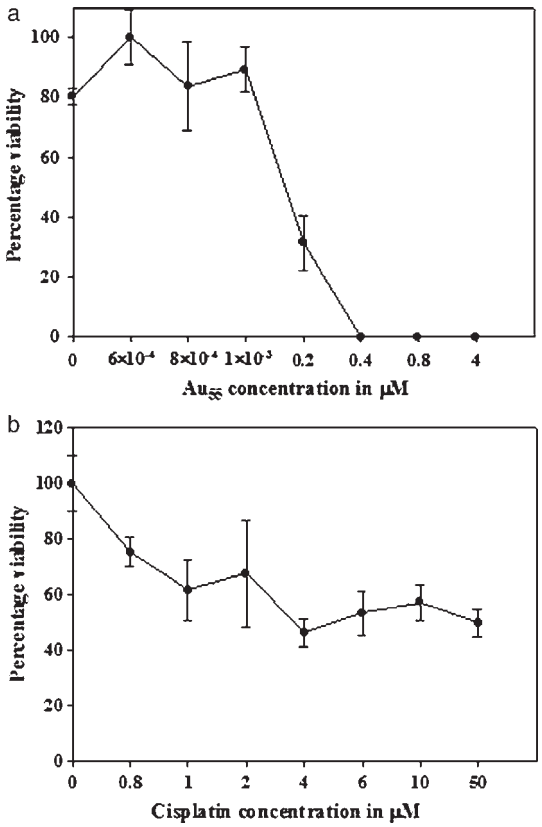

Fig. 36 Viability of melanoma cells in dependence of concentration of $Au_{55}(Ph_2PC_6H_4SO_3H)_{12}Cl_6$ (a) and cisplatin (b). (Reprinted with permission from ref. 74. Copyright 2005, Wiley-VCH.).

From Fig. 36 the result for the BLM cells is presented in a visualized form.

Whereas for the Au_{55} particles the viability zero is already reached with 0.4 μM amount, in case of cisplatin viability is still 50% even with 50 μM amount of the complex.

The distribution of gold in various parts of the cells was determined in case of the BLM melanoma cells using radioanalysis. Cell fragmentations and successive neutron

Table 2 IC_{50} values of 11 human cancer cell lines using cisplatin (72 h) and Au_{55} (24 h)

		IC_{50}/μM	
Cell line	Type	Cisplatin, 72 h	Au_{55}, 24 h
MC3T3-E1	Bone cells	26.10 ± 1.27	1.65 ± 0.14
U-2OS	Osteosarcoma	11.17 ± 2.02	0.64 ± 0.04
SK-ES-1	Osteosarcoma	0.79 ± 0.17	1.03 ± 0.18
MOR/P	Lung cancer cells	3.30 ± 0.30	2.10 ± 0.10
MOR/CPR	Lung cancer cells	7.10 ± 1.2	2.50 ± 0.10
CCD-919Sk	Fibroblast cells	0.45 ± 0.10	0.62 ± 0.07
BLM	Metastatic melanoma	54.70 ± 7.60	0.30 ± 0.10
MV3	Metastatic melanoma	> 50	0.24 ± 0.02
SK-Mel-28	Melanoma	15.60 ± 2.26	1.12 ± 016
HeLa	Cervical cancer cells	7.93 ± 0.95	2.29 ± 0.10
Hek-12	Kidney cancer cells transformed with adenovirus	20.13 ± 6.0	0.63 ± 0.02

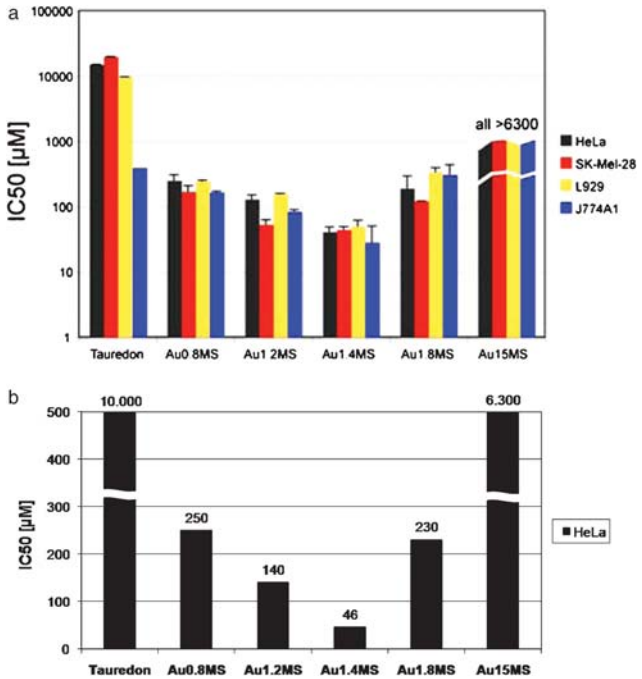

Fig. 37 (a) Comparison of IC_{50} values of four different cell lines using different gold nanoparticles and the complex Tauredon in logarithmic scaling. Abbreviations: *e.g.* Au0.8MS = 0.8 nm Au particle, stabilized by MS (monosulfonated triphenylphosphine). ((a) Reprinted with permission from ref. 75. Copyright 2007, Wiley-VCH). (b) Linear scaling of the HeLa values.

irradiation allowed very exact [^{198}Au]gold radioanalysis with the result found that 20–25% of the gold was associated with DNA, a very high value, supporting the *in vitro* experiments.

The exceptional position of Au_{55} in cytotoxicity has impressively been confirmed by comparing smaller and larger gold nanoparticles with Au_{55}, all equipped with the same kind of sulfonated triphenylphosphines as ligand molecules. IC_{50} values of four cell lines, namely HeLa, SK-Mel-28, L929 and J774A1, have been determined in parallel using Tauredon, a commercially available gold thiomalate complex, 0.8 nm (Au_9), 1.2 nm, 1.4 nm (Au_{55}), 1.8 nm and 15 nm particles, all stabilized by $Ph_2PC_6H_4SO_3Na$.[75] Fig. 37(a) shows the results.

For the first time a well expressed size-dependent cytotoxicity of gold nanoparticles is shown. The maximum toxicity is found for Au_{55} in all four cases. Only slightly smaller (1.2 nm) or larger (1.8 nm) particles exhibit a remarkable increase of the IC_{50} values and herewith a corresponding decrease of toxicity. The Au complex Tauredon and the 15 nm gold particles do not indicate measurable toxicity. The difference in cytotoxicity between Au_{55} and the smaller and larger particles becomes even more impressive in Fig. 37(b), where a linear correlation between the different toxicities in case of the HeLa cell lines is shown.

The very important role of the phosphine ligands as weakly coordinated molecules becomes obvious by using the 0.8 nm and the 1.4 nm clusters, stabilized by glutathione ligands instead of phosphines. Very stable Au–S bonds prevent ligand dissociation with the consequence of absolute non-toxicity! These experiments prove that gold nanoparticles only become toxic if available in bare form, or rather provided with ligands that are easily substituted.

It is still an open question if the differences in toxicity, especially between the particles with only small variations in size, are due to a perfect (Au_{55}) or a less good fit (1.2 nm, 1.8 nm) to the major grooves of DNA, or if a different mechanism of chemical destruction of the cells is responsible. Indeed, the latter may be more likely, since it was shown that Au_{55} and 1.2 nm particles cause a different kind of cell death. Whereas Au_{55} clearly induces necrosis, the 1.2 nm and 1.8 nm particles initiate apoptotic cell death.[75] Of course, these two results are only first hints that different particle–cell interactions may happen, even with such small differences in particle size. It can also not be excluded that the observed very fast cell death using Au_{55} is exclusively due to interactions with DNA. Other decisive destructive interactions may also occur.

5. Conclusions and outlook

The two-shell cluster Au_{55}, existing with various ligand shells and in bare form, has attracted unusual attention for several reasons. There is the perfect cuboctahedral geometry (which is inherent in any other full-shell cluster), being responsible for an extraordinary stability, which is especially observable in the chemical inertness of the Au_{55} nucleus and in its ability to become organized in three-dimensional architectures. Even more attractive from a scientific, but also from a practical point of view, is the extraordinary electronic situation in $Au_{55}(PPh_3)_{12}Cl_6$. Numerous different physical methods indicate that this cluster compound exactly meets the borderline between bulk materials and molecules and so behaves as a typical quantum dot. Bulk as well as molecular behaviour can be observed, depending on the criteria and method applied. The cluster's capability to be switched by single electrons at room temperature belongs probably to the most important findings. First steps to use this unique property for applications in future nanoelectronic devices have been made. However, it is clearly a substantial challenge to realise this possible goal.

Independent of the special electronic quality of Au_{55}, a more accidental effect opened another door of application, namely in toxicology and medicine.

Based on the findings that the Au_{55} nucleus with its 1.4 nm diameter and the height of the major groove of DNA fit perfectly to each other and that the presence of several phosphate groups around the groove coordinate the gold nanoparticle in the manner of a multidentate ligand, a series of cell experiments were carried out. Indeed, it seems realistic that this irreversible connection between Au_{55} and DNA is at least one explanation for the extraordinary cytotoxicity, observed for more than a dozen human cancer cell lines. This assumption is supported by the fact that slightly smaller or larger gold nanoparticles show drastically lower toxicity and by the observation that Au_{55} induces necrosis, whereas 1.2 nm and 1.8 nm particles cause apoptosis.

As yet there are no data on the specificity of Au_{55}, *i.e.* the ratio of toxicity of tumor cells and healthy cells. Even if this ratio was high, long-term study and development, as for using Au_{55} as a single electron switch in future storage systems, would be required to make Au_{55} a successful anti-cancer drug. Hopes in both cases seem justified.

References

1 G. Schmid, R. Boese, R. Pfeil, F. Bandermann, S. Mayer, G. H. M. Calis and J. W. A. van der Velden, *Chem. Ber*., 1981, **114**, 3634.
2 M. Faraday, *Philos. Trans. R. Soc. London*, 1861, **151**, 183.
3 J. P. Wilcoxon and B. L. Abrams, *Chem. Soc. Rev*., 2006, **35**, 1162.
4 M.-C. Daniel and D. Astruc, *Chem. Rev*., 2004, **104**, 293.
5 J. W. A. van der Velden, J. J. Bour, W. P. Bosman and J. H. Hoordik, *J. Chem. Soc., Chem. Commun*., 1981, 1218.
6 P. L. Bellon, F. Cariati, M. Manassero, L. Naldini and M. Sansoni, *J. Chem. Soc. D*, 1971, 1423.
7 K. P. Hall, B. R. C. Theobald, D. I. Gilmour, D. M. P. Mingos and A. J. Welch, *J. Chem. Soc., Chem. Commun*., 1982, 528.
8 C. E. Briant, K. P. Hall, A. C. Wheeler and D. M. P. Mingos, *J. Chem. Soc., Chem. Commun*., 1984, 248.
9 M. McPartlin, R. Mason and L. Malatesta, *J. Chem. Soc. D*, 1969, 334.
10 G. Albano, P. L. Bellon, M. Manassero and M. Sansoni, *J. Chem. Soc. D*, 1970, 1210.
11 L. Bellon, M. Manassero and M. Sansoni, *J. Chem. Soc., Dalton Trans*., 1972, 1481.
12 J. W. A. van der Velden, F. A. Vollenbroek, J. J. Bour, P. I. Beurskens, J. M. M. Smits and W. P. Bosman, *Recl.: J. R. Neth. Chem. Soc*., 1981, **100**, 148.
13 B. K. Teo, X. Shi and H. Zhang, *J. Am. Chem. Soc*., 1992, **114**, 2743.
14 P. D. Jadzinsky, G. Calero, C. J. Ackerson, D. A. Bushnell and R. D. Kornberg, *Science*, 2007, **318**, 430.
15 O. Echt, K. Sattler and E. Recknagel, *Phys. Rev. Lett*., 1981, **47**, 1121.
16 V. G. Albano, A. Ceriotti, P. Chini, G. Ciani, S. Martinengo and W. M. Anker, *J. Chem. Soc., Chem. Commun*., 1975, 859.
17 G. Schmid, U. Giebel, W. Huster and A. Schwenk, *Inorg. Chim. Acta*, 1984, **85**, 97.
18 G. Schmid, B. Morun and J.-O. Malm, *Angew. Chem., Int. Ed. Engl*., 1989, **28**, 778.
19 G. Schmid, N. Klein, B. Morun and A. Lehnert, *Pure Appl. Chem*., 1990, **62**, 1175.
20 G. Schmid, M. Harms, J.-O. Malm, J.-O. Bovin, J. van Ruitenbeck, H. W. Zandbergen and W. T. Fu, *J. Am. Chem. Soc*., 1993, **115**, 2046.
21 C. E. Briant, B. R. C. Theobald, J. W. White, L. K. Bell and D. M. P. Mingos, *J. Chem. Soc., Chem. Commun*., 1981, 201.
22 G. Schmid, *Inorg. Synth*., 1990, **7**, 214.
23 G. Schmid, *Chem. Rev*., 1985, **62**, 51.
24 G. Schmid, N. Klein, L. Korste, U. Kreibig and D. Schönauer, *Polyhedron*, 1988, **7**, 605.
25 G. Schmid, R. Pugin, W. Meyer-Zaika and U. Simon, *Eur. J. Inorg. Chem*., 1999, 2051.
26 G. Schmid, R. Pugin, J.-O. Malm and J.-O. Bovin, *Eur. J. Inorg. Chem*., 1998, 813.
27 W. M. Pankau, S. Mönninghoff and G. von Kiedrowski, *Angew. Chem., Int. Ed*., 2006, **45**, 1889.
28 G. Schmid, R. Pugin, T. Sawitowski, U. Simon and B. Marler, *Chem. Commun*., 1999, 1303.
29 N. Beyer, Diploma Thesis, University of Essen, 1997.
30 G. Schmid and N. Beyer, *Eur. J. Inorg. Chem*., 2000, 835.
31 G. Schmid, M. Bäumle and N. Beyer, *Angew. Chem., Int. Ed*., 2000, **39**, 181.
32 O. Vidoni, T. Reuter, V. Torma, W. Meyer-Zaika and G. Schmid, *J. Mater. Chem*., 2001, **11**, 3188.
33 R. Maoz, S. R. Cohen and J. Sagiv, *Adv. Mater*., 1999, **11**, 55.
34 R. Maoz, E. Frydman, S. R. Cohen and J. Sagiv, *Adv. Mater*., 2000, **12**, 424.
35 R. Maoz, E. Frydman, S. R. Cohen and J. Sagiv, *Adv. Mater*., 2000, **12**, 725.
36 S. Liu, R. Maoz, G. Schmid and J. Sagiv, *Nano Lett*., 2002, **2**, 1055.
37 G. Schmid and N. Klein, *Angew. Chem., Int. Ed. Engl*., 1986, **25**, 922.
38 H. Feld, A. Leute, D. Rading, A. Benninghoven and G. Schmid, *J. Am. Chem. Soc*., 1990, **112**, 8166.
39 G. Schmid, W. Meyer-Zaika, R. Pugin, T. Sawitowski, J.-P. Majoral, A.-M. Caminade and C.-O. Turrin, *Chem.–Eur. J*., 2000, **6**, 1693.
40 G. Schmid, E. Emmrich, J.-P. Majoral and A.-M. Caminade, *Small*, 2005, **1**, 73.
41 H.-G. Boyen, G. Kästle, F. Weigl, B. Koslowski, C. Dietrich, P. Ziemann, J. P. Spatz, S. Riethmüller, C. Hartmann, M. Möller, G. Schmid, M. G. Garnier and P. Oelhafen, *Science*, 2002, **297**, 1533.
42 M. Comotti, C. Della Pina and R. Matarrese M. Rossi, *Angew. Chem., Int. Ed*., 2004, **43**, 5812.
43 H.-G. Boyen, A. Ethirajan, G. Kästle, F. Weigl, P. Ziemann, G. Schmid, M. G. Garnier, M. Büttner and P. Oelhafen, *Appl. Phys. Lett*., 2005, **94**, 016804-1.
44 H. Brune, H. Ernst, A. Grunwald, W. Grünwald, H. Hofmann, H. Krug, P. Janich, M. Major, W. Rathgeber, G. Schmid, U. Simon, V. Vogel and D. Wyrwa, in *Nanotechnology. Assessment and Perspectives*, ed. C. F. Gethmann, Springer, Berlin, Heidelberg, 2006.
45 B. A. Smith, J. Z. Zhang, U. Giebel and G. Schmid, *Chem. Phys. Lett*., 1997, **270**, 139.
46 K. Fauth, U. Kreibig and G. Schmid, *Z. Phys. D: At., Mol. Clusters*, 1991, **20**, 297.
47 H. H. A. Smit, R. C. Thiel, L. J. de Jongh, G. Schmid and N. Klein, *Solid State Commun*., 1988, **65**, 915.
48 P. D. Cluskey, R. J. Newport, R. E. Benfield, S. J. Gurman and G. Schmid, *Z. Phys. D: At., Mol. Clusters*, 1993, **26**, 8.
49 A. Bezryadin, C. Dekker and G. Schmid, *Appl. Phys. Lett*., 1997, **71**, 1273.
50 J. G. A. Dubois, J. W. Gerritsen, S. E. Shafranjuk, E. J. G. Boon, G. Schmid and H. van Kempen, *Europhys. Lett*., 1996, **33**, 279.
51 L. F. Chi, M. Hartig, T. Drechsler, T. Schwaak, C. Seidel, H. Fuchs and G. Schmid, *Appl. Phys. A: Mater. Sci. Process*., 1998, **66**, 187.
52 H. Zhang, U. Hartmann and G. Schmid, *Appl. Phys. Lett*., 2004, **84**, 1543.
53 H. Zhang, G. Schmid and U. Hartmann, *Nano Lett*., 2003, **3** 305.
54 U. Simon, G. Schön and G. Schmid, *Angew. Chem., Int. Ed. Engl*., 1993, **32**, 250.
55 G. Schön and U. Simon, *Colloid Polym. Sci*., 1995, **273**, 101.
56 G. Schön and U. Simon, *Colloid Polym. Sci*., 1995, **273**, 202.
57 G. Schmid and U. Simon, *Chem. Commun*., 2005, 697.
58 Y. Liu, M. Schumann, T. Raschke, C. Radehaus and G. Schmid, *Nano Lett*., 2001, **1**, 405.
59 V. Torma, G. Schmid and U. Simon, *ChemPhysChem*, 2001, **2**, 321.
60 O. Vidoni, S. Neumeier, N. Bardou, J.-L. Pelouard and G. Schmid, *J. Cluster Sci*., 2003, **14**, 325.
61 T. Reuter, S. Neumeier, G. Schmid, E. Koplin and U. Simon, *Eur. J. Inorg. Chem*., 2005, 3670.
62 S. Neumeier, T. Reuter and G. Schmid, *Eur. J. Inorg. Chem*., 2005, 3679.
63 V. Torma, T. Reuter, O. Vidoni, M. Schumann, C. Radehaus and G. Schmid, *ChemPhysChem*, 2001, **2**, 546.
64 G. Moore, *Electronics*, 1965, 3.
65 G. Schmid, T. Reuter, U. Simon, M. Noyong, K. Blech, V. Santhanam, D. Jäger, H. Slomka, H. Lüth and M. I. Lepsa, *Colloid Polym. Sci*., 2008, **286**, 1029.
66 E. C. Connor, J. Mwamuka, A. Gole, C. J. Murphy and M. D. Wyatt, *Small*, 2005, **1**, 325.
67 B. D. Chitrani, A. A. Ghazani and W. C. W. Chan, *Nano Lett*., 2006, **6**, 662.
68 R. Shukla, V. Bansal, M. Chaudhary, A. Basu, R. R. Bhonde and M. Sastry, *Langmuir*, 2005, **21**, 10644.
69 A. G. Tkachenko, H. Xie, Y. Liu, D. Coleman, J. Ryan, W. R. Glomm, M. K. Shipton, S. Franzen and D. L. Feldheim, *Bioconjugate Chem*., 2004, **15**, 482.
70 N. Pernodet, X. Fang, Y. Sun, A. Bakhtina, A. Ramakrishnan, J. Sokolov, A. Ulman and M. Rafailovich, *Small*, 2006, **2**, 766.
71 C. M. Goodman, C. D. McCusker, T. Yilmaz and V. M. Rotello, *Bioconjugate Chem*., 2004, **15**, 897.
72 Y. Liu, W. Meyer-Zaika, S. Franzka, G. Schmid, M. Tsoli and H. Kuhn, *Angew. Chem., Int. Ed*., 2003, **42**, 2853.
73 *Oxford Handbook of Nucleic Acid Structure*, ed. S. Neidle, Oxford University Press, New York, 1999.
74 M. Tsoli, H. Kuhn, W. Brandau, H. Esche and G. Schmid, *Small*, 2005, **1**, 841.
75 Y. Pan, S. Neuss, A. Leifert, M. Fischler, F. Wen, U. Simon, G. Schmid, W. Brandau and W. Jahnen-Dechent, *Small*, 2007, **3**, 1941.